

Di-Higgs production as a probe of flavor changing neutral Yukawa couplings

Shi-Ping He^{1,*}

¹*Center for Future High Energy Physics and Theoretical Physics Division,
Institute of High Energy Physics, Chinese Academy of Sciences, Beijing 100049, China*
(Dated: December 8, 2020)

Top partners are well motivated in many new physics models. Usually, vector like quarks $T_{L,R}$ are introduced to avoid the quantum anomaly. It is crucial to probe their interactions with the standard model particles. However, flavor changing neutral couplings are always difficult to detect directly in the current and future experiments. In this paper, we will show how to constrain the flavor changing neutral Yukawa coupling Tth through the di-Higgs production indirectly. We consider the simplified model including a pair of gauge singlet $T_{L,R}$. Under the perturbative unitarity and experimental constraints, we choose $m_T = 400$ GeV, $s_L = 0.2$ and $m_T = 800$ GeV, $s_L = 0.1$ as benchmark points. After the analysis of amplitude and evaluation of the numerical cross sections, we find that the present constraints from di-Higgs production have already surpassed the unitarity bound because of the $(y_{L,R}^{tT})^4$ behavior. For the case of $m_T = 400$ GeV and $s_L = 0.2$, $\text{Re}y_{L,R}^{tT}$ and $\text{Im}y_{L,R}^{tT}$ can be bounded optimally in the range $(-0.4, 0.4)$ at HL-LHC with 2σ CL. For the case of $m_T = 800$ GeV and $s_L = 0.1$, $\text{Re}y_{L,R}^{tT}$ and $\text{Im}y_{L,R}^{tT}$ can be bounded optimally in the range $(-0.5, 0.5)$ at HL-LHC with 2σ CL. The anomalous triple Higgs coupling δ_{hhh} can also affect the constraints on $y_{L,R}^{tT}$. Finally, we find that the top quark electric dipole moment can give stronger bounds of $y_{L,R}^{tT}$ in the off-axis regions for some scenarios.

CONTENTS

I. Introduction	2
II. Framework of flavor changing neutral couplings	3
II.1. Minimal singlet vector-like quark model	3
II.2. Simplified model	3
III. Constraints on the simplified model	4
IV. The analysis of double Higgs production	6
IV.1. New physics results of the amplitude	6
IV.2. Heavy quark expansion	10
IV.3. The cross section analysis	10
V. The numerical results and constraint prospects	11
V.1. The benchmark point $m_T = 400$ GeV and $s_L = 0.2$	13
V.2. The benchmark point $m_T = 800$ GeV and $s_L = 0.1$	14
V.3. Comments on the doublet and triplet vector-like quarks	16

* sphe@ihep.ac.cn

VI. Summary and conclusions	18
Acknowledgements	19
References	19
Appendix	23
A. Asymptotic behaviors of the loop functions	23
A.1. The shorthand notations of C_0 and D_0 functions	23
A.2. Heavy quark expansion of C_0 function	24
A.3. Heavy quark expansion of D_0 function	27

I. INTRODUCTION

The standard model (SM) of elementary particle physics has been proposed for more than fifty years [1], and it is proved to be a very effective description of this field [2]. The electro-weak symmetry breaking (EWSB) [3] mechanism predicts the existence of a physical Higgs boson, which is observed at the Large Hadron Collider (LHC) in 2012 [4]. Although the SM goes such strong, there are still some clouds in the sky of particle physics. The typical problems are Higgs mass naturalness, gauge coupling unification, fermion mass hierarchy, electro-weak vacuum stability, dark matter, matter anti-matter asymmetry, and so on. Many new physics beyond the SM (BSM) are aimed at solving or partially solving these problems. In some of these BSM models, vector-like quarks (VLQs)[5, 6] are introduced to avoid the quantum anomaly.

For the up-type VLQ, the T quark can interact with the SM particles via the TbW , TtZ , and Tth interactions. Constraints on these couplings are crucial, because they may help us unveil the nature of the EWSB. For the strong interaction mediated pair production of VLQs, we can only constrain the partial decay branching ratios of the T quark. To bound these couplings, single production of VLQ needs to be considered. Unfortunately, it is difficult to detect the flavor changing neutral (FCN) interactions TtZ , Tth directly because of the suppression of the single T production from tZ , th fusion. Here, we will focus on the FCN Yukawa (FCNY) interaction Tth . After the Higgs boson discovery, we can get more and more information on new physics from the Higgs precision measurements [7]. The FCNY interaction can show up in loop induced processes, for example $h \rightarrow \gamma Z$ and $gg \rightarrow hh$. In our previous work [8], we show that it is possible to constrain the FCNY coupling through the $h \rightarrow \gamma Z$ decay mode indirectly. The double Higgs production is also an appealing channel for unravelling the FCNY interaction, which is free of electro-weak gauge interactions. The constraints from $h \rightarrow \gamma Z$ and $gg \rightarrow hh$ are independent of exotic decay modes and total width of the T quark.

In this paper, we build the framework of FCN couplings in Sec. II first. Sec. III is devoted to the theoretical and experimental constraints on the simplified model. In Sec. IV, we compute the new physics contributions to the parton level cross section of $gg \rightarrow hh$. Then we perform the numerical constraints on the FCNY interactions in Sec. V. Finally, we give the summary and conclusions in Sec. VI.

II. FRAMEWORK OF FLAVOR CHANGING NEUTRAL COUPLINGS

II.1. Minimal singlet vector-like quark model

The SM gauge group is $SU_C(3) \otimes SU_L(2) \otimes U_Y(1)$, under which the singlet up-type VLQs have the representation $(3, 0, 2/3)$. Let us start with the minimal extension of SM by adding a pair of singlet T_L, T_R [5, 6], which is named as the VLQT model. Note that the mass mixing term $\bar{T}_L t_R$ can be eliminated with field redefinition [9, 10]. Then, the Lagrangian can be written as [6]

$$\begin{aligned} \mathcal{L} &= \mathcal{L}_{SM} + \mathcal{L}_T^{Yukawa} + \mathcal{L}_T^{gauge}, \\ \mathcal{L}_T^{Yukawa} &= -\Gamma_T^i \bar{Q}_L^i \tilde{\Phi} T_R - M_T \bar{T}_L T_R + \text{h.c.}, \quad \mathcal{L}_T^{gauge} = \bar{T}_L i\cancel{D} T_L + \bar{T}_R i\cancel{D} T_R, \end{aligned} \quad (1)$$

where $\tilde{\Phi} = i\sigma_2 \Phi^*$ and the covariant derivative is defined as $D_\mu = \partial_\mu - ig' Y_T B_\mu$. Y_T and Q_T are the $U_Y(1)$ and electric charge of the T quark, respectively. The Higgs doublet is parametrized as $\Phi^T = [\phi^+, \frac{v+h+ix}{\sqrt{2}}]$. It is reasonable to neglect the mixings between heavy particles and the first two generations because of mass hierarchy and the bounds from flavor physics [11–13]. Here, we only consider the mixings between the third generation and heavy quarks for simplicity.

To diagonalize the t and T quark mass terms, we can perform the transformations

$$\begin{bmatrix} t_L \\ T_L \end{bmatrix} \rightarrow \begin{bmatrix} \cos \theta_L & \sin \theta_L \\ -\sin \theta_L & \cos \theta_L \end{bmatrix} \begin{bmatrix} t_L \\ T_L \end{bmatrix}, \quad \begin{bmatrix} t_R \\ T_R \end{bmatrix} \rightarrow \begin{bmatrix} \cos \theta_R & \sin \theta_R \\ -\sin \theta_R & \cos \theta_R \end{bmatrix} \begin{bmatrix} t_R \\ T_R \end{bmatrix}. \quad (2)$$

In fact, we have the relation $m_T \tan \theta_R = m_t \tan \theta_L$. In the following, we will take s_L, c_L, s_R, c_R as shorthands for $\sin \theta_L, \cos \theta_L, \sin \theta_R, \cos \theta_R$, respectively. Then, we can obtain the mass eigenstate Yukawa interactions

$$\mathcal{L}_{Yukawa} \supset -m_t \bar{t}t - m_T \bar{T}T - \frac{m_t}{v} c_L^2 h \bar{t}t - \frac{m_T}{v} s_L^2 h \bar{T}T - \frac{m_T}{v} s_L c_L h (\bar{t}_L T_R + \bar{T}_R t_L) - \frac{m_t}{v} s_L c_L h (\bar{T}_L t_R + \bar{t}_R T_L), \quad (3)$$

and gauge interactions

$$\begin{aligned} \mathcal{L}_{gauge} &\supset \frac{g}{c_W} Z_\mu \left[\left(\frac{1}{2} c_L^2 - \frac{2}{3} s_W^2 \right) \bar{t}_L \gamma^\mu t_L + \left(\frac{1}{2} s_L^2 - \frac{2}{3} s_W^2 \right) \bar{T}_L \gamma^\mu T_L + \frac{1}{2} s_L c_L (\bar{t}_L \gamma^\mu t_L + \bar{T}_L \gamma^\mu t_L) \right. \\ &\quad \left. - \frac{2}{3} s_W^2 \bar{t}_R \gamma^\mu t_R - \frac{2}{3} s_W^2 \bar{T}_R \gamma^\mu T_R \right] + \frac{gc_L}{\sqrt{2}} (W_\mu^+ \bar{t}_L \gamma^\mu b_L + W_\mu^- \bar{b}_L \gamma^\mu t_L) + \frac{gs_L}{\sqrt{2}} (W_\mu^+ \bar{T}_L \gamma^\mu b_L + W_\mu^- \bar{b}_L \gamma^\mu T_L). \end{aligned} \quad (4)$$

Here, we have two independent extra parameters m_T and θ_L . For more details, please refer to our previous work [8].

II.2. Simplified model

Besides the singlet VLQs, the scalar sector can also be enlarged in the non-minimally extended models. For example, we can also introduce a real gauge singlet scalar [14, 15], a Higgs doublet [16], and even both the singlet-doublet scalars at the same time [16, 17]. In these models, the T

quark can exist other decay channels [18, 19]. Here, we will adopt a general framework [20]. Then, the simplified related mass eigenstate interactions can be read as [8]

$$\begin{aligned} \mathcal{L} \supset & -m_t \bar{t}t - m_T \bar{T}T - e A_\mu \sum_{f=t,T} Q_f \bar{f} \gamma^\mu f + e Z_\mu [\bar{t} \gamma^\mu (g_L^t \omega_- + g_R^t \omega_+) t + \bar{T} \gamma^\mu (g_L^T \omega_- + g_R^T \omega_+) T \\ & + \bar{t} \gamma^\mu (g_L^{tT} \omega_- + g_R^{tT} \omega_+) T + \bar{T} \gamma^\mu (g_L^{tT} \omega_- + g_R^{tT} \omega_+) t] - \frac{m_t}{v} h \bar{t} (\kappa_t + i \gamma^5 \tilde{\kappa}_t) t + h \bar{T} (y_T + i \gamma^5 \tilde{y}_T) T \\ & + h \bar{t} (y_L^{tT} \omega_- + y_R^{tT} \omega_+) T + h \bar{T} ((y_L^{tT})^* \omega_+ + (y_R^{tT})^* \omega_-) t + \frac{g c_L}{\sqrt{2}} (W_\mu^+ \bar{t}_L \gamma^\mu b_L + W_\mu^- \bar{b}_L \gamma^\mu t_L) \\ & + \frac{g s_L}{\sqrt{2}} (W_\mu^+ \bar{T}_L \gamma^\mu b_L + W_\mu^- \bar{b}_L \gamma^\mu T_L) - \lambda_{hhh} h^3, \end{aligned} \quad (5)$$

where ω_\pm are the chirality projection operators $(1 \pm \gamma^5)/2$ and the gauge couplings are listed as

$$\begin{aligned} g_L^t &= \frac{1}{s_W c_W} \left(\frac{1}{2} c_L^2 - \frac{2}{3} s_W^2 \right), \quad g_L^T = \frac{1}{s_W c_W} \left(\frac{1}{2} s_L^2 - \frac{2}{3} s_W^2 \right), \quad g_L^{tT} = \frac{s_L c_L}{2 s_W c_W}, \\ g_R^t &= -\frac{2 s_W}{c_W}, \quad g_R^T = -\frac{2 s_W}{c_W}, \quad g_R^{tT} = 0. \end{aligned} \quad (6)$$

The triple Higgs coupling λ_{hhh} can deviate from the SM value $\lambda_{hhh}^{SM} = \frac{m_h^2}{2v}$ in many new physics models [21–30]. Here, $m_T, \theta_L, \kappa_t, \tilde{\kappa}_t, y_T, \tilde{y}_T$ are all real parameters, while y_L^{tT}, y_R^{tT} can be complex. From now on, we will turn off the parameters $\tilde{\kappa}_t$ and \tilde{y}_T for simplicity.

In the following context, we will show how to constrain the FCNY couplings through the $gg \rightarrow hh$ channel. Although the FCNY couplings $y_{L,R}^{tT}$ are not free parameters in the above VLQT model, they can be free in more complex models. If we can extend the SM by the singlet T_L, T_R and many new scalars, there can be enough degrees of freedom. Thus, we can take them as free parameters to make a general analysis.

III. CONSTRAINTS ON THE SIMPLIFIED MODEL

In this section, we will review the theoretical and experimental constraints on the simplified model. Specific details are already given in our previous study [8]. S -wave unitarity will lead to the bound [8]

$$\sqrt{(|y_L^{tT}|^2 + |y_R^{tT}|^2)^2 + 12|y_L^{tT}|^2|y_R^{tT}|^2} + |y_L^{tT}|^2 + |y_R^{tT}|^2 \leq 16\pi. \quad (7)$$

In Fig. 1, we show the unitarity allowed region in the plane of $|y_L^{tT}| - |y_R^{tT}|$. Higgs signal strength and top quark physics give quite loose constraints. Direct search can bound the VLQ mass as light as 400 GeV without specific assumptions [19]. The strongest constraints on m_T and s_L come from the electro-weak precision measurements. Here, we consider the S and T parameters [13, 31–34]. In Fig. 2, we show the allowed parameter space regions from the global fits at 1σ and 2σ confidence level (CL). In this paper, the input parameters are chosen as $m_Z = 91.1876$ GeV, $m_W = 80.387$ GeV, $m_h = 125.09$ GeV, $m_t = 172.74$ GeV, $G_F = 1.1664 \times 10^{-5}$ GeV $^{-2}$, and $c_W = m_W/m_Z$ [2].

Then, we turn to the constraints from the top quark electric dipole moment (EDM) [35–39]. If there exists CP violation in the FCNY interactions, it will contribute to the EDM type interaction $-\frac{i}{2} d_t^{EDM} \bar{t} \sigma^{\mu\nu} \gamma^5 t F_{\mu\nu}$. The d_t^{EDM} is computed as

$$d_t^{EDM} = \frac{e Q_T m_T [y_R^{tT} (y_L^{tT})^* - y_L^{tT} (y_R^{tT})^*]}{16\pi^2} C_1, \quad (8)$$

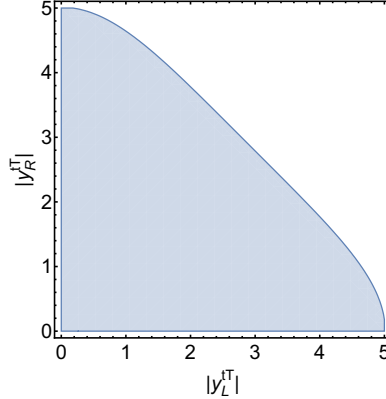
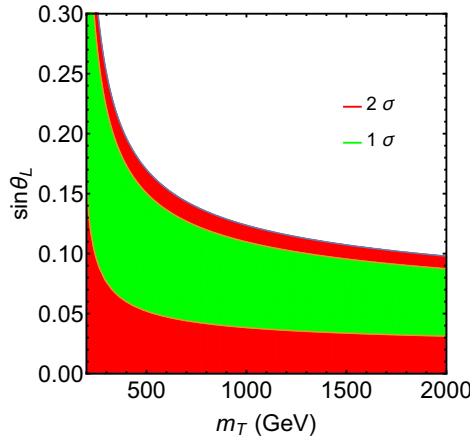


FIG. 1. The region allowed by the perturbative unitarity.

FIG. 2. The constraints on m_T, s_L from the S and T parameters. Here, the green and red label the allowed regions at 1σ and 2σ CL, respectively.

with C_1 defined as

$$C_1 = \frac{1}{4m_t^2} [B_0(m_t^2, m_T^2, m_h^2) - B_0(0, m_T^2, m_T^2) + (m_T^2 - m_t^2 - m_h^2) C_0(m_t^2, 0, m_t^2, m_h^2, m_T^2, m_T^2)].$$

As can be seen from the identity $[y_R^{tT}(y_L^{tT})^* - y_L^{tT}(y_R^{tT})^*] = 2i(\text{Re}y_L^{tT}\text{Im}y_R^{tT} - \text{Re}y_R^{tT}\text{Im}y_L^{tT})$, d_t^{EDM} will vanish if the imaginary parts of $y_{L,R}^{tT}$ are both turned off. If we take $m_T = 400$ GeV, top EDM sets the upper limit of $|y_R^{tT}(y_L^{tT})^* - y_L^{tT}(y_R^{tT})^*|$ to be 0.12 at 90% CL. If we take $m_T = 800$ GeV, the corresponding upper limit of $|y_R^{tT}(y_L^{tT})^* - y_L^{tT}(y_R^{tT})^*|$ is 0.24 at 90% CL. The larger m_T is, the looser will the constraints be.

IV. THE ANALYSIS OF DOUBLE HIGGS PRODUCTION

IV.1. New physics results of the amplitude

The double Higgs production is a hot topic in the field of Higgs physics. The di-Higgs production cross section has been calculated in SM for many years [40, 41]. The new physics effects have also drawn much attention of this community [42–46]. Some works on di-Higgs production are based on the SM effective field theory (EFT) [47–52] and non-linearly realized EFT [53–56]. There are also many studies considered in specific models, for example, Higgs singlet model [57–59], two Higgs doublet model [60–63], VLQ models [64–66], composite Higgs models [67, 68], minimal supersymmetric standard model (MSSM) [69–71], next-to-MSSM [72, 73], and many other new physics models.

For VLQ models, there are additional fermion contributions: the pure new quark loops and the loops with both SM and new quarks. In Fig. 3 and Fig. 4, we show the Feynman diagrams from the pure quark loops and mixed quark loops, respectively ¹. The latter will be induced by the FCNY interactions. The FCNY contributions are less considered in most of the studies, because they are small compared to the same flavor terms. As a second thought, this channel can be sensitive to large FCNY couplings.

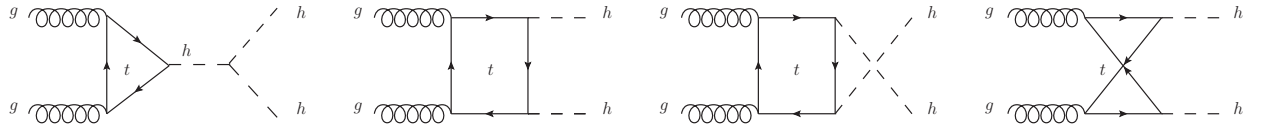


FIG. 3. Typical Feynman diagrams contributing to the $g(k_1, \mu)g(k_2, \nu) \rightarrow h(p_1)h(p_2)$ production with pure top (also T) quarks running in the loops, where the counter-clockwise diagrams should be included.

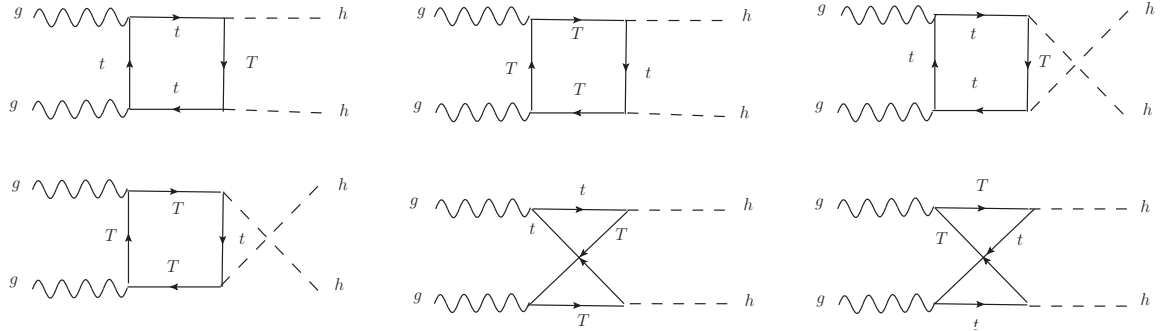


FIG. 4. Typical Feynman diagrams contributing to the $g(k_1, \mu)g(k_2, \nu) \rightarrow h(p_1)h(p_2)$ production with both top and T quarks running in the loops, where the counter-clockwise diagrams should be included.

¹ The diagrams are drawn by JaxoDraw [74].

Starting from the Lagrangian in Eq. (5), the amplitude of $gg \rightarrow hh$ can be parametrized as

$$i\mathcal{M}(\hat{s}) = -i \frac{g_s^2 \hat{s}}{16\pi^2 v^2} \epsilon_\mu^{a,r_1}(k_1) \epsilon_\nu^{a,r_2}(k_2) (A^{\mu\nu} f_A + B^{\mu\nu} f_B + C^{\mu\nu} f_C), \quad (9)$$

where a and $r_{1,2}$ are the color and spin indices, and the tensor structures $A^{\mu\nu}$, $B^{\mu\nu}$, $C^{\mu\nu}$ are given by

$$\begin{aligned} A^{\mu\nu} &\equiv g^{\mu\nu} - \frac{k_2^\mu k_1^\nu}{k_1 \cdot k_2}, & C^{\mu\nu} &\equiv \frac{k_{1\rho} k_{2\sigma} \epsilon^{\mu\nu\rho\sigma}}{k_1 \cdot k_2}, \\ B^{\mu\nu} &\equiv g^{\mu\nu} + \frac{m_h^2 k_2^\mu k_1^\nu}{p_T^2 (k_1 \cdot k_2)} - \frac{2(k_1 \cdot p_1) k_2^\mu p_1^\nu}{p_T^2 (k_1 \cdot k_2)} - \frac{2(k_2 \cdot p_1) p_1^\mu k_1^\nu}{p_T^2 (k_1 \cdot k_2)} + \frac{2p_1^\mu p_1^\nu}{p_T^2} & (p_T^2 &\equiv \frac{\hat{t}\hat{u} - m_h^4}{\hat{s}}). \end{aligned} \quad (10)$$

They have the orthonormal relations $A^{\mu\nu} A_{\mu\nu} = B^{\mu\nu} B_{\mu\nu} = C^{\mu\nu} C_{\mu\nu} = 2$ and $A^{\mu\nu} B_{\mu\nu} = A^{\mu\nu} C_{\mu\nu} = B^{\mu\nu} C_{\mu\nu} = 0$. The coefficients $f_{A,B,C}$ receive contributions from the t and T quark loops. They can be written as $f_{A,B,C} \equiv f_{A,B,C}^t + f_{A,B,C}^T + f_{A,B,C}^{tT}$. Here $f_{A,B,C}^{t(T)}$ mark the contributions from pure $t(T)$ quark loops, while $f_{A,B,C}^{tT}$ labels the contributions from mixed t and T quark loops. When we set $\kappa_t^2 = 1$ and turn off the couplings $y_{L,R}^{tT}$, they will go to the SM result. After some lengthy calculations, we can obtain their explicit expressions.

The pure top quark contribution to f_A is given by² $f_A^t = \kappa_t f_A^{t,\Delta} + \kappa_t^2 f_A^{t,\square 1}$. Here, $f_A^{t,\Delta}$ and $f_A^{t,\square 1}$ are defined as

$$\begin{aligned} f_A^{t,\Delta} &= \frac{6m_h^2 m_t^2}{\hat{s}(\hat{s} - m_h^2)} [2 + (4m_t^2 - \hat{s}) C_0^t(\hat{s})], \\ f_A^{t,\square 1} &= \frac{2m_t^2}{\hat{s}} \left\{ 4m_t^2 C_0^t(\hat{s}) + \frac{2(m_h^2 - 4m_t^2)}{\hat{s}} [(t - m_h^2) C_0^t(t) + (\hat{u} - m_h^2) C_0^t(\hat{u})] \right. \\ &\quad \left. + m_t^2 (8m_t^2 - \hat{s} - 2m_h^2) [D_0^t(t, \hat{s}) + D_0^t(\hat{u}, \hat{s}) + D_0^t(t, \hat{u})] + 2 + \frac{\hat{t}\hat{u} - m_h^4}{\hat{s}} (4m_t^2 - m_h^2) D_0^t(t, \hat{u}) \right\}. \end{aligned} \quad (11)$$

The pure T quark contribution to f_A is given by $f_A^T = (-\frac{vy_T}{m_T}) f_A^{T,\Delta} + (\frac{vy_T}{m_T})^2 f_A^{T,\square 1}$. Here, $f_A^{T,\Delta}$ and $f_A^{T,\square 1}$ are defined as

$$\begin{aligned} f_A^{T,\Delta} &= \frac{6m_h^2 m_T^2}{\hat{s}(\hat{s} - m_h^2)} [2 + (4m_T^2 - \hat{s}) C_0^T(\hat{s})], \\ f_A^{T,\square 1} &= \frac{2m_T^2}{\hat{s}} \left\{ 4m_T^2 C_0^T(\hat{s}) + \frac{2(m_h^2 - 4m_T^2)}{\hat{s}} [(t - m_h^2) C_0^T(t) + (\hat{u} - m_h^2) C_0^T(\hat{u})] \right. \\ &\quad \left. + m_T^2 (8m_T^2 - \hat{s} - 2m_h^2) [D_0^T(t, \hat{s}) + D_0^T(\hat{u}, \hat{s}) + D_0^T(t, \hat{u})] + 2 + \frac{\hat{t}\hat{u} - m_h^4}{\hat{s}} (4m_T^2 - m_h^2) D_0^T(t, \hat{u}) \right\}. \end{aligned} \quad (12)$$

The top and T quark mixed contribution to f_A is given by $f_A^{tT} = (|y_L^{tT}|^2 + |y_R^{tT}|^2) f_A^{tT,\square 1} + [y_L^{tT} (y_R^{tT})^* +$

² During the calculations, we have used the FeynCalc to simplify the results [75, 76].

$y_R^{tT}(y_L^{tT})^*[f_A^{tT,\square 2}]$. Here, $f_A^{tT,\square 1}$ and $f_A^{tT,\square 2}$ are defined as

$$\begin{aligned}
& f_A^{tT,\square 1} \\
&= \frac{2v^2}{\hat{s}} \left\{ 2m_t^2 C_0^t(\hat{s}) + 2m_T^2 C_0^T(\hat{s}) + \frac{m_h^2 - m_t^2 - m_T^2}{\hat{s}} [(\hat{t} - m_h^2)(C_0^{tT}(\hat{t}) + C_0^{Tt}(\hat{t})) + (\hat{u} - m_h^2)(C_0^{tT}(\hat{u}) + C_0^{Tt}(\hat{u}))] \right. \\
&\quad + (m_t^2 + m_T^2 - m_h^2)[m_t^2(D_0^{tT}(\hat{t}, \hat{s}) + D_0^{tT}(\hat{u}, \hat{s}) + D_0^{tT}(\hat{t}, \hat{u})) + m_T^2(D_0^{Tt}(\hat{t}, \hat{s}) + D_0^{Tt}(\hat{u}, \hat{s}) + D_0^{Tt}(\hat{t}, \hat{u}))] \\
&\quad \left. + 2 + \frac{\hat{t}\hat{u} - m_h^4}{\hat{s}}(m_t^2 + m_T^2 - m_h^2)D_0^{tT}(\hat{t}, \hat{u}) \right\}, \\
& f_A^{tT,\square 2} = \frac{m_t m_T v^2}{\hat{s}^2} \left\{ 4(m_h^2 - \hat{t})(C_0^{tT}(\hat{t}) + C_0^{Tt}(\hat{t})) + 4(m_h^2 - \hat{u})(C_0^{tT}(\hat{u}) + C_0^{Tt}(\hat{u})) \right. \\
&\quad + \hat{s}(4m_t^2 - \hat{s})[D_0^{tT}(\hat{t}, \hat{s}) + D_0^{tT}(\hat{u}, \hat{s}) + D_0^{tT}(\hat{t}, \hat{u})] + \hat{s}(4m_T^2 - \hat{s})[D_0^{Tt}(\hat{t}, \hat{s}) + D_0^{Tt}(\hat{u}, \hat{s}) + D_0^{Tt}(\hat{t}, \hat{u})] \\
&\quad \left. + 4(\hat{t}\hat{u} - m_h^4)D_0^{tT}(\hat{t}, \hat{u}) \right\}. \tag{13}
\end{aligned}$$

The pure top quark contribution to f_B is given by $f_B^t = \kappa_t^2 f_B^{t,\square 1}$. Here, $f_B^{t,\square 1}$ is defined as

$$\begin{aligned}
& f_B^{t,\square 1} = \frac{m_t^2}{\hat{s}} \left\{ -2\hat{s}C_0^t(\hat{s}) + 2(m_h^2 - \hat{t})C_0^t(\hat{t}) + 2(m_h^2 - \hat{u})C_0^t(\hat{u}) - 2(8m_t^2 + \hat{s} - 2m_h^2)C_0^t(m_h^2) \right. \\
&\quad + 2m_t^2(8m_t^2 + \hat{s} - 2m_h^2)[D_0^t(\hat{t}, \hat{s}) + D_0^t(\hat{u}, \hat{s}) + D_0^t(\hat{t}, \hat{u})] \\
&\quad + \frac{1}{\hat{t}\hat{u} - m_h^4} \left[\hat{s}\hat{t}(8m_t^2\hat{t} - \hat{t}^2 - m_h^4)D_0^t(\hat{t}, \hat{s}) + \hat{s}\hat{u}(8m_t^2\hat{u} - \hat{u}^2 - m_h^4)D_0^t(\hat{u}, \hat{s}) \right. \\
&\quad \left. + (8m_t^2 + \hat{s} - 2m_h^2) \left(\hat{s}(\hat{s} - 2m_h^2)C_0^t(\hat{s}) + \hat{s}(\hat{s} - 4m_h^2)C_0^t(m_h^2) + 2\hat{t}(m_h^2 - \hat{t})C_0^t(\hat{t}) + 2\hat{u}(m_h^2 - \hat{u})C_0^t(\hat{u}) \right) \right] \right\}. \tag{14}
\end{aligned}$$

The pure T quark contribution to f_B is given by $f_B^T = (\frac{vy_T}{m_T})^2 f_B^{T,\square 1}$. Here, $f_B^{T,\square 1}$ is defined as

$$\begin{aligned}
& f_B^{T,\square 1} = \frac{m_T^2}{\hat{s}} \left\{ -2\hat{s}C_0^T(\hat{s}) + 2(m_h^2 - \hat{t})C_0^T(\hat{t}) + 2(m_h^2 - \hat{u})C_0^T(\hat{u}) - 2(8m_T^2 + \hat{s} - 2m_h^2)C_0^T(m_h^2) \right. \\
&\quad + 2m_T^2(8m_T^2 + \hat{s} - 2m_h^2)[D_0^T(\hat{t}, \hat{s}) + D_0^T(\hat{u}, \hat{s}) + D_0^T(\hat{t}, \hat{u})] \\
&\quad + \frac{1}{\hat{t}\hat{u} - m_h^4} \left[\hat{s}\hat{t}(8m_T^2\hat{t} - \hat{t}^2 - m_h^4)D_0^T(\hat{t}, \hat{s}) + \hat{s}\hat{u}(8m_T^2\hat{u} - \hat{u}^2 - m_h^4)D_0^T(\hat{u}, \hat{s}) \right. \\
&\quad \left. + (8m_T^2 + \hat{s} - 2m_h^2) \left(\hat{s}(\hat{s} - 2m_h^2)C_0^T(\hat{s}) + \hat{s}(\hat{s} - 4m_h^2)C_0^T(m_h^2) + 2\hat{t}(m_h^2 - \hat{t})C_0^T(\hat{t}) + 2\hat{u}(m_h^2 - \hat{u})C_0^T(\hat{u}) \right) \right] \right\}. \tag{15}
\end{aligned}$$

The top and T quark mixed contribution to f_B is given by $f_B^{tT} = (|y_L^{tT}|^2 + |y_R^{tT}|^2)f_B^{tT,\square 1} + [y_L^{tT}(y_R^{tT})^* +$

$y_R^{tT}(y_L^{tT})^*[f_B^{tT,\square 2}]$. Here, $f_B^{tT,\square 1}$ is defined as

$$\begin{aligned}
& f_B^{tT,\square 1} \\
&= \frac{2v^2}{\hat{s}} \left\{ -\frac{\hat{s}}{2}[C_0^t(\hat{s}) + C_0^T(\hat{s})] - \frac{1}{2}(\hat{s} - 2m_h^2 + 2m_t^2 + 2m_T^2)[C_0^{tT}(m_h^2) + C_0^{Tt}(m_h^2)] + \frac{m_h^2 - \hat{t}}{2}[C_0^{tT}(t) + C_0^{Tt}(t)] \right. \\
&+ \frac{m_h^2 - \hat{u}}{2}[C_0^{tT}(u) + C_0^{Tt}(u)] + \frac{1}{2}(m_t^2 - m_T^2)(\hat{s} + m_t^2 + m_T^2 - m_h^2)[D_0^{tT}(\hat{t}, \hat{s}) + D_0^{tT}(\hat{u}, \hat{s}) - D_0^{Tt}(\hat{t}, \hat{s}) - D_0^{Tt}(\hat{u}, \hat{s})] \\
&+ \frac{(m_t^2 + m_T^2)}{4}(\hat{s} - 2m_h^2 + 2m_t^2 + 2m_T^2)[D_0^{tT}(\hat{t}, \hat{s}) + D_0^{tT}(\hat{u}, \hat{s}) + D_0^{Tt}(\hat{t}, \hat{u}) + D_0^{Tt}(\hat{u}, \hat{s}) + D_0^{Tt}(\hat{t}, \hat{u})] \\
&+ \frac{1}{4(\hat{t}\hat{u} - m_h^4)} \left[\hat{s}(\hat{s} - 2m_h^2)(\hat{s} - 2m_h^2 + 2m_t^2 + 2m_T^2)[C_0^t(\hat{s}) + C_0^T(\hat{s})] \right. \\
&+ 2\hat{s}(m_T^2 - m_t^2)(\hat{s} - 2m_h^2 + 2m_t^2 + 2m_T^2)[C_0^t(\hat{s}) - C_0^T(\hat{s})] + \hat{s}(\hat{s} - 4m_h^2)(\hat{s} - 2m_h^2 + 2m_t^2 + 2m_T^2)[C_0^{tT}(m_h^2) + C_0^{Tt}(m_h^2)] \\
&+ 2\hat{t}(m_h^2 - \hat{t})(\hat{s} - 2m_h^2 + 2m_t^2 + 2m_T^2)[C_0^{tT}(\hat{t}) + C_0^{Tt}(\hat{t})] + 2\hat{u}(m_h^2 - \hat{u})(\hat{s} - 2m_h^2 + 2m_t^2 + 2m_T^2)[C_0^{tT}(\hat{u}) + C_0^{Tt}(\hat{u})] \\
&+ \hat{s}(m_t^2 - m_T^2)^2(\hat{s} - 2m_h^2 + 2m_t^2 + 2m_T^2)[D_0^{tT}(\hat{t}, \hat{s}) + D_0^{tT}(\hat{u}, \hat{s}) + D_0^{Tt}(\hat{t}, \hat{u}) + D_0^{Tt}(\hat{t}, \hat{s}) + D_0^{Tt}(\hat{u}, \hat{s}) + D_0^{Tt}(\hat{t}, \hat{u})] \\
&+ 2\hat{s}\hat{t}(m_t^2 - m_T^2)(\hat{s} - 2m_h^2 + 2m_t^2 + 2m_T^2)[D_0^{tT}(\hat{t}, \hat{s}) - D_0^{Tt}(\hat{t}, \hat{s})] \\
&+ 2\hat{s}\hat{u}(m_t^2 - m_T^2)(\hat{s} - 2m_h^2 + 2m_t^2 + 2m_T^2)[D_0^{tT}(\hat{u}, \hat{s}) - D_0^{Tt}(\hat{u}, \hat{s})] \\
&\left. - \hat{s}\hat{t}(\hat{t}^2 + m_h^4 - 2\hat{t}(m_t^2 + m_T^2)) \left(D_0^{tT}(\hat{t}, \hat{s}) + D_0^{tT}(\hat{u}, \hat{s}) \right) - \hat{s}\hat{u}(\hat{u}^2 + m_h^4 - 2\hat{u}(m_t^2 + m_T^2)) \left(D_0^{Tt}(\hat{t}, \hat{s}) + D_0^{Tt}(\hat{u}, \hat{s}) \right) \right], \tag{16}
\end{aligned}$$

and $f_B^{tT,\square 2}$ is defined as

$$\begin{aligned}
& f_B^{tT,\square 2} = \frac{2m_t m_T v^2}{\hat{s}} \left\{ -2[C_0^{tT}(m_h^2) + C_0^{Tt}(m_h^2)] + 2m_t^2[D_0^{tT}(\hat{t}, \hat{s}) + D_0^{tT}(\hat{u}, \hat{s}) + D_0^{tT}(\hat{t}, \hat{u})] \right. \\
&+ 2m_T^2[D_0^{Tt}(\hat{t}, \hat{s}) + D_0^{Tt}(\hat{u}, \hat{s}) + D_0^{Tt}(\hat{t}, \hat{u})] + \frac{1}{\hat{t}\hat{u} - m_h^4} \left[\hat{s}(\hat{s} - 2m_h^2)[C_0^t(\hat{s}) + C_0^T(\hat{s})] - 2\hat{s}(m_t^2 - m_T^2)[C_0^t(\hat{s}) - C_0^T(\hat{s})] \right. \\
&+ \hat{s}(\hat{s} - 4m_h^2)[C_0^{tT}(m_h^2) + C_0^{Tt}(m_h^2)] + 2\hat{t}(m_h^2 - \hat{t})[C_0^{tT}(\hat{t}) + C_0^{Tt}(\hat{t})] + 2\hat{u}(m_h^2 - \hat{u})[C_0^{tT}(\hat{u}) + C_0^{Tt}(\hat{u})] \\
&+ \hat{s}(\hat{t}^2 + (m_t^2 - m_T^2)^2)[D_0^{tT}(\hat{t}, \hat{s}) + D_0^{tT}(\hat{t}, \hat{u})] + \hat{s}(\hat{u}^2 + (m_t^2 - m_T^2)^2)[D_0^{tT}(\hat{u}, \hat{s}) + D_0^{tT}(\hat{u}, \hat{u})] \\
&\left. + 2\hat{s}\hat{t}(m_t^2 - m_T^2)[D_0^{tT}(\hat{t}, \hat{s}) - D_0^{tT}(\hat{t}, \hat{u})] + 2\hat{s}\hat{u}(m_t^2 - m_T^2)[D_0^{tT}(\hat{u}, \hat{s}) - D_0^{tT}(\hat{u}, \hat{u})] + 2\hat{s}(m_t^2 - m_T^2)^2 D_0^{tT}(\hat{t}, \hat{u}) \right], \tag{17}
\end{aligned}$$

The pure top quark contribution to f_C is proportional to $\tilde{\kappa}_t$, so we set f_C^t to be zero. Similarly, the pure T quark contribution to f_C is also turned off. The top and T quark mixed contribution to f_C is given by $f_C^{tT} = -i[y_L^{tT}(y_R^{tT})^* - y_R^{tT}(y_L^{tT})^*]f_C^{tT,\square}$. Here, $f_C^{tT,\square}$ is defined as

$$f_C^{tT,\square} = m_t m_T v^2 [D_0^{tT}(\hat{t}, \hat{s}) + D_0^{tT}(\hat{u}, \hat{s}) + D_0^{tT}(\hat{t}, \hat{u}) + D_0^{Tt}(\hat{t}, \hat{s}) + D_0^{Tt}(\hat{u}, \hat{s}) + D_0^{Tt}(\hat{t}, \hat{u})]. \tag{18}$$

IV.2. Heavy quark expansion

In the limit of $\frac{m_h^2, \hat{s}, \hat{t}, \hat{u}}{m_t^2} \ll 1$, the coefficients of pure top quark loops f_A^t, f_B^t, f_C^t can be expanded as

$$\begin{aligned} f_A^{t,\triangle} &= \frac{2m_h^2}{\hat{s} - m_h^2} \left[1 + \frac{7\hat{s}}{120m_t^2} + \mathcal{O}\left(\frac{1}{m_t^4}\right) \right], \quad f_A^{t,\square 1} = -\frac{2}{3} \left[1 + \frac{7m_h^2}{20m_t^2} + \mathcal{O}\left(\frac{1}{m_t^4}\right) \right], \\ f_B^{t,\square 1} &= \frac{11(m_h^4 - \hat{t}\hat{u})}{90m_t^2\hat{s}} + \mathcal{O}\left(\frac{1}{m_t^4}\right), \quad f_B^{t,\square 2} = \frac{m_h^4 - \hat{t}\hat{u}}{6m_t^2\hat{s}} + \mathcal{O}\left(\frac{1}{m_t^4}\right), \\ f_C^{t,\triangle} &= \frac{3m_h^2}{\hat{s} - m_h^2} \left[1 + \frac{\hat{s}}{12m_t^2} + \mathcal{O}\left(\frac{1}{m_t^4}\right) \right], \quad f_C^{t,\square} = -2 \left[1 + \frac{m_h^2}{3m_t^2} + \mathcal{O}\left(\frac{1}{m_t^4}\right) \right]. \end{aligned} \quad (19)$$

For the coefficients of pure T quark loops, they are just the ones with m_t replaced by m_T .

For the case of t and T quark mixed loops, things are more complicated. In the limit of $\frac{m_h^2, \hat{s}, \hat{t}, \hat{u}}{m_{t,T}^2} \ll 1$, the coefficient $f_A^{tT}, f_B^{tT}, f_C^{tT}$ can be expanded as

$$\begin{aligned} f_A^{tT,\square 1} &= \mathcal{O}\left(\frac{1}{m_{t,T}^4}\right), \\ f_B^{tT,\square 1} &= \frac{v^2(\hat{t}^2 - \hat{u}^2)}{m_T^2(\hat{t}\hat{u} - m_h^4)} \cdot \frac{(1 + r_{tT}^2)(1 + 2r_{tT}^2 \log r_{tT}^2 - r_{tT}^4)}{2r_{tT}^2(1 - r_{tT}^2)^2} + \mathcal{O}\left(\frac{1}{m_{t,T}^4}\right), \\ f_C^{tT,\square} &= \frac{v^2}{m_t m_T} + \mathcal{O}\left(\frac{1}{m_{t,T}^4}\right). \end{aligned} \quad (20)$$

IV.3. The cross section analysis

When averaging the initial spin and color degrees of freedom, we can get the partonic cross section of $gg \rightarrow hh$ at leading order (LO) as follows

$$\begin{aligned} \hat{\sigma}_{LO}(gg \rightarrow hh; \hat{s}) &= \frac{\alpha_S^2 G_F^2 \sqrt{\hat{s}(\hat{s} - 4m_h^2)}}{128(4\pi)^3} \int_{-1}^1 d\cos\theta (|f_A|^2 + |f_B|^2 + |f_C|^2) \\ &= \frac{\alpha_S^2 G_F^2}{64(4\pi)^3} \int_{\hat{t}_{min}}^{\hat{t}_{max}} d\hat{t} (|f_A|^2 + |f_B|^2 + |f_C|^2) (\hat{t}_{min} = -\frac{1}{4}(\sqrt{\hat{s}} + \sqrt{\hat{s} - 4m_h^2})^2, \hat{t}_{max} = -\frac{1}{4}(\sqrt{\hat{s}} - \sqrt{\hat{s} - 4m_h^2})^2), \end{aligned} \quad (21)$$

where f_A, f_B, f_C are calculated as

$$\begin{aligned} f_A &= f_A^t + f_A^T + f_A^{tT} = \kappa_t f_A^{t,\triangle} + \kappa_t^2 f_A^{t,\square 1} + \left(-\frac{vy_T}{m_T}\right) f_A^{T,\triangle} + \left(\frac{vy_T}{m_T}\right)^2 f_A^{T,\square 1} \\ &\quad + (|y_L^{tT}|^2 + |y_R^{tT}|^2) f_A^{tT,\square 1} + [y_L^{tT} (y_R^{tT})^* + y_R^{tT} (y_L^{tT})^*] f_A^{tT,\square 2}, \\ f_B &= f_B^t + f_B^T + f_B^{tT} = \kappa_t^2 f_B^{t,\square 1} + \left(\frac{vy_T}{m_T}\right)^2 f_B^{T,\square 1} + (|y_L^{tT}|^2 + |y_R^{tT}|^2) f_B^{tT,\square 1} + [y_L^{tT} (y_R^{tT})^* + y_R^{tT} (y_L^{tT})^*] f_B^{tT,\square 2}, \\ f_C &= f_C^t + f_C^T + f_C^{tT} = -i[y_L^{tT} (y_R^{tT})^* - y_R^{tT} (y_L^{tT})^*] f_C^{tT,\square}. \end{aligned} \quad (22)$$

Note that there is a $\frac{1}{2}$ factor in the partonic cross section because of the identical final states. In general, the anomalous triple Higgs coupling λ_{hhh} will also alter the di-Higgs production cross section. Its effects can be captured with $f_A^{f,\Delta}, f_C^{f,\Delta}$ ($f = t, T$) multiplied by the factor $1 + \delta_{hhh} \equiv \lambda_{hhh}/\lambda_{hhh}^{SM}$.

After folding the partonic cross section with the gluon luminosity, we can get the hadron level cross section

$$\sigma_{LO}(pp \rightarrow hh) = \int_{\frac{4m_h^2}{s}}^1 d\tau \int_\tau^1 \frac{dx}{x} f(x, \mu_F^2) f(\frac{\tau}{x}, \mu_F^2) \hat{\sigma}_{LO}(gg \rightarrow hh; \hat{s} = \tau s), \quad (23)$$

where f represents the gluon parton distribution function (PDF) and μ_F is the factorization scale.

V. THE NUMERICAL RESULTS AND CONSTRAINT PROSPECTS

Just similar to the VLQT model, we take $\kappa_t = c_L^2, y_T = -\frac{m_T}{v} s_L^2$ for simplicity, but let $\text{Re}(y_L^{tT}), \text{Re}(y_R^{tT}), \text{Im}(y_L^{tT}), \text{Im}(y_R^{tT})$ to be free. Then we can choose several benchmark scenarios and estimate the constraints on the magnitude and sign of the FCNY couplings. Now, we need to normalize the cross section to the SM ones numerically for fixed m_T and s_L , which is defined as

$$\mu_{hh} \equiv \frac{\sigma_{LO}(pp \rightarrow hh)}{\sigma_{LO}^{SM}(pp \rightarrow hh)}. \quad (24)$$

Up to LO level, μ_{hh} can be parametrized as

$$\begin{aligned} \mu_{hh} = & 1 + A_1 + A_0^{hhh} \delta_{hhh} + A_1^{hhh} \delta_{hhh}^2 + (A_2 + A_2^{hhh} \delta_{hhh})(|y_L^{tT}|^2 + |y_R^{tT}|^2) \\ & + (A_3 + A_3^{hhh} \delta_{hhh})[y_L^{tT}(y_R^{tT})^* + y_R^{tT}(y_L^{tT})^*] + A_4(|y_L^{tT}|^2 + |y_R^{tT}|^2)^2 + A_5[y_L^{tT}(y_R^{tT})^* + y_R^{tT}(y_L^{tT})^*]^2 \\ & + A_6(|y_L^{tT}|^2 + |y_R^{tT}|^2)[y_L^{tT}(y_R^{tT})^* + y_R^{tT}(y_L^{tT})^*] - A_7[y_L^{tT}(y_R^{tT})^* - y_R^{tT}(y_L^{tT})^*]^2, \end{aligned} \quad (25)$$

From the observation of Eq. (21) and Eq. (22), we can find that $A_1, A_2, A_3, A_0^{hhh}, A_1^{hhh}, A_2^{hhh}, A_3^{hhh}$ depend on the choices of both m_T and s_L , while A_4, A_5, A_6, A_7 only depend on m_T . Moreover, A_1^{hhh}, A_4, A_5, A_7 are always non-negative and A_1 vanishes as s_L goes to zero.

Although $\sigma^{SM}(pp \rightarrow hh)$ has been calculated with high precision [77–85], we will not do that hard work here. We only keep the LO results because a large part of the QCD corrections can be cancelled in the ratio [48, 56, 86, 87]. To get the numerical results of cross sections, we write a model file through FeynRules [88, 89], FeynArts [90] and NLOCT [91]. Then it is linked to MadGraph [92]. Before the numerical calculations, we take the following default settings:

- Proton contains b, \bar{b} , that is, we use the 5FS (5 flavor scheme).
- We adopt the PDF choice of "MSTW2008lo68cl" (LHAPDF ID 21000).
- The default *dynamical_scale_choice* is set to be 3 (see [93]).
- The input parameters are choose as $m_h = 125.09$ GeV, $G_F = 1.1664 \times 10^{-5}$ GeV $^{-2}$, $m_t = 172.74$ GeV, and $\alpha_s(m_Z) = 0.1184$. Thus we have $v = 246.221$ GeV.

Currently, the Higgs pair production is bounded to be $|\mu_{hh}| \leq 6.9$ at 95% confidence level (CL) [94, 95]. At the high luminosity LHC (HL-LHC), di-Higgs production measurement is accessible. The expected signal strength is $\mu_{hh} = 1.00^{+0.41}_{-0.39}$ with 1σ uncertainty [96]. We take the benchmark points as $m_T = 400$ GeV, $s_L = 0.2$ and $m_T = 800$ GeV, $s_L = 0.1$, and all the following discussions are based on the two benchmark points. Now, we should determine the specific values of $A_1, A_2, A_3, A_4, A_5, A_6, A_7$ and $A_0^{hhh}, A_1^{hhh}, A_2^{hhh}, A_3^{hhh}$. First of all, we have $\sigma_{LO}^{SM}(pp \rightarrow hh) =$

24.7 fb. When setting different values of $\delta_{hh}, y_L^{tT}, y_R^{tT}$, we can obtain different normalized cross sections (see Tab. I and Tab. II). Then the numerical values of A_1, \dots, A_7 and $A_0^{hhh}, A_1^{hhh}, A_2^{hhh}, A_3^{hhh}$ can be solved from the first seven and last four equations individually. Their results are given in Tab. III.

δ_{hh}	(y_L^{tT}, y_R^{tT})	expressions of μ_{hh}	numerical values of μ_{hh}
0	(0, 0)	$1 + A_1$	0.8081
	(0, 1)	$1 + A_1 + A_2 + A_4$	1.254
	(0, $\frac{1}{2}$)	$1 + A_1 + \frac{1}{4}A_2 + \frac{1}{16}A_4$	0.9057
	(1, 1)	$1 + A_1 + 2A_2 + 2A_3 + 4A_4 + 4A_5 + 4A_6$	10.92
	(1, -1)	$1 + A_1 + 2A_2 - 2A_3 + 4A_4 + 4A_5 - 4A_6$	1.695
	(1, i)	$1 + A_1 + 2A_2 + 4A_4 + 4A_7$	14.13
	($\frac{1}{2}$, $\frac{1}{2}$)	$1 + A_1 + \frac{1}{2}A_2 + \frac{1}{2}A_3 + \frac{1}{4}A_4 + \frac{1}{4}A_5 + \frac{1}{4}A_6$	2.206
1	(0, 0)	$1 + A_1 + A_0^{hhh} + A_1^{hhh}$	0.3877
	(0, 1)	$1 + A_1 + A_0^{hhh} + A_1^{hhh} + A_2 + A_2^{hhh} + A_4$	0.6996
	(1, 1)	$1 + A_1 + A_0^{hhh} + A_1^{hhh} + 2(A_2 + A_2^{hhh}) + 2(A_3 + A_3^{hhh}) + 4A_4 + 4A_5 + 4A_6$	8.235
-1	(0, 0)	$1 + A_1 - A_0^{hhh} + A_1^{hhh}$	1.779

TABLE I. The normalized cross sections for different $\delta_{hh}, y_L^{tT}, y_R^{tT}$ values with $m_T = 400$ GeV and $s_L = 0.2$ at $\sqrt{s}=14\text{TeV}$.

δ_{hh}	(y_L^{tT}, y_R^{tT})	expressions of μ_{hh}	numerical values of μ_{hh}
0	(0, 0)	$1 + A_1$	0.9506
	(0, 1)	$1 + A_1 + A_2 + A_4$	1.098
	(0, $\frac{1}{2}$)	$1 + A_1 + \frac{1}{4}A_2 + \frac{1}{16}A_4$	0.9838
	(1, 1)	$1 + A_1 + 2A_2 + 2A_3 + 4A_4 + 4A_5 + 4A_6$	5.255
	(1, -1)	$1 + A_1 + 2A_2 - 2A_3 + 4A_4 + 4A_5 - 4A_6$	0.3376
	(1, i)	$1 + A_1 + 2A_2 + 4A_4 + 4A_7$	5.247
	($\frac{1}{2}$, $\frac{1}{2}$)	$1 + A_1 + \frac{1}{2}A_2 + \frac{1}{2}A_3 + \frac{1}{4}A_4 + \frac{1}{4}A_5 + \frac{1}{4}A_6$	1.675
1	(0, 0)	$1 + A_1 + A_0^{hhh} + A_1^{hhh}$	0.4502
	(0, 1)	$1 + A_1 + A_0^{hhh} + A_1^{hhh} + A_2 + A_2^{hhh} + A_4$	0.5526
	(1, 1)	$1 + A_1 + A_0^{hhh} + A_1^{hhh} + 2(A_2 + A_2^{hhh}) + 2(A_3 + A_3^{hhh}) + 4A_4 + 4A_5 + 4A_6$	3.519
-1	(0, 0)	$1 + A_1 - A_0^{hhh} + A_1^{hhh}$	2.013

TABLE II. The normalized cross sections for different $\delta_{hh}, y_L^{tT}, y_R^{tT}$ values with $m_T = 800$ GeV and $s_L = 0.1$ at $\sqrt{s}=14\text{TeV}$.

\sqrt{s} (TeV)	$(m_T/\text{GeV}, s_L)$	A_1	A_2	A_3	A_4	A_5	A_6	A_7
14	(400, 0.2)	-0.1919	0.3717	1.672	0.07449	1.114	0.3166	3.071
	(800, 0.1)	-0.04939	0.1279	1.087	0.01943	0.378	0.0711	0.9907
\sqrt{s} (TeV)	$(m_T/\text{GeV}, s_L)$	A_0^{hhh}	A_1^{hhh}	A_2^{hhh}	A_3^{hhh}			
14	(400, 0.2)	-0.6958	0.2754	-0.1343	-0.9956			
	(800, 0.1)	-0.7814	0.281	-0.04494	-0.5731			

TABLE III. The coefficients in Eq. (25) solved through the signal strength values in Tab. I and Tab. II.

V.1. The benchmark point $m_T = 400$ GeV and $s_L = 0.2$

For the case of $m_T = 400$ GeV and $s_L = 0.2$, the numerical results of μ_{hh} are evaluated as

$$\begin{aligned} \mu_{hh} = & 1 - 0.1919 - 0.6958 \delta_{hhh} + 0.2754 \delta_{hhh}^2 + (0.3717 - 0.1343 \delta_{hhh})(|y_L^{tT}|^2 + |y_R^{tT}|^2) \\ & + (1.672 - 0.9956 \delta_{hhh})[y_L^{tT}(y_R^{tT})^* + y_R^{tT}(y_L^{tT})^*] + 0.07449(|y_L^{tT}|^2 + |y_R^{tT}|^2)^2 + 1.114[y_L^{tT}(y_R^{tT})^* + y_R^{tT}(y_L^{tT})^*]^2 \\ & + 0.3166(|y_L^{tT}|^2 + |y_R^{tT}|^2)[y_L^{tT}(y_R^{tT})^* + y_R^{tT}(y_L^{tT})^*] - 3.071[y_L^{tT}(y_R^{tT})^* - y_R^{tT}(y_L^{tT})^*]^2. \end{aligned} \quad (26)$$

In this case, the present di-Higgs production experiments give the constraints $\delta_{hhh} \in (-3.61, 6.13)$ and $\text{Re}y_L^{tT}, \text{Im}y_L^{tT}, \text{Re}y_R^{tT}, \text{Im}y_R^{tT} \in (-2.62, 2.62)$ at 95% CL by setting one parameter at a time. In Tab. IV, we give the expected constraints on the parameters $\delta_{hhh}, \text{Re}y_L^{tT}, \text{Im}y_L^{tT}, \text{Re}y_R^{tT}, \text{Im}y_R^{tT}$ at HL-LHC. It can be seen that both of the current and expected constraints at HL-LHC are stronger than the unitarity bound, the reason is that the highest power in di-Higgs production cross section is proportional to $(y_{L,R}^{tT})^4$.

parameters		δ_{hhh}	$\text{Re}y_L^{tT}$	$\text{Im}y_L^{tT}$	$\text{Re}y_R^{tT}$	$\text{Im}y_R^{tT}$
individual	1 σ	(-0.681, 0.327) \cup (2.20, 3.21)	(-1.13, 1.13)	(-1.13, 1.13)	(-1.13, 1.13)	(-1.13, 1.13)
	2 σ	(-1.03, 3.56)	(-1.40, 1.40)	(-1.40, 1.40)	(-1.40, 1.40)	(-1.40, 1.40)
marginalized	1 σ	(-3.76, 3.99)	(-1.91, 1.91)	(-1.91, 1.91)	(-1.91, 1.91)	(-1.91, 1.91)
	2 σ	(-4.48, 4.66)	(-2.09, 2.09)	(-2.09, 2.09)	(-2.09, 2.09)	(-2.09, 2.09)

TABLE IV. The expected 1σ and 2σ bounds at HL-LHC for the parameters $\delta_{hhh}, \text{Re}y_L^{tT}, \text{Im}y_L^{tT}, \text{Re}y_R^{tT}, \text{Im}y_R^{tT}$ under the benchmark point $m_T = 400$ GeV and $s_L = 0.2$. Here we adopt two different methods: (1) turn on one parameter at a time, namely the individual method; (2) turn on all the five parameters, namely the marginalized method.

As mentioned above, there are four interesting parameters $\text{Re}(y_L^{tT}), \text{Re}(y_R^{tT}), \text{Im}(y_L^{tT}), \text{Im}(y_R^{tT})$. Then we can plot the reached two-dimensional parameter space by setting two of them to be zero or imposing two conditions. Here we choose six scenarios: ① $y_{L,R}^{tT}$ are both real (it is similar to the both imaginary number case); ② y_R^{tT} is real and y_L^{tT} is imaginary (it is similar to the real y_R^{tT} and imaginary y_L^{tT} case); ③ $y_R^{tT} = 0$ (similar to the $y_L^{tT} = 0$ case); ④ $y_L^{tT} = y_R^{tT}$; ⑤ $y_L^{tT} = -y_R^{tT}$; ⑥ $y_L^{tT} = (y_R^{tT})^*$.

In Fig. 5 and Fig. 6, we show the plots with $\delta_{hhh} = 0$ and $\delta_{hhh} = 0.5$, respectively. From these plots, we find that $\text{Re}(y_{L,R}^{tT})$ and $\text{Im}(y_{L,R}^{tT})$ are constrained to be in the range $(-2, 2)$ roughly at 2σ CL. In some of these scenarios, the 2σ interval can be tight as $(-0.4, 0.4)$. The reach regions of 1σ and 2σ are quite different. The value of δ_{hhh} has significant effects on the extraction of $y_{L,R}^{tT}$. For the first (upper left) plot, the first and third quadrants are more constrained. This can

be understood from the Eq. (22), because there is constructive interference between the positive $[y_L^{tT}(y_R^{tT})^* + y_R^{tT}(y_L^{tT})^*]$ term and other box diagram induced terms. While it is destructive interference if $[y_L^{tT}(y_R^{tT})^* + y_R^{tT}(y_L^{tT})^*]$ is negative. The last five plots are symmetric with respect to the horizontal and vertical axes. For the second (upper central) and sixth (lower right) plots, they receive the contributions from the $[y_L^{tT}(y_R^{tT})^* - y_R^{tT}(y_L^{tT})^*]$ term. Because $|f_C|^2$ in Eq. (21) is always positive, the constraints are stronger. For the fourth (lower left) plot, positive $[y_L^{tT}(y_R^{tT})^* + y_R^{tT}(y_L^{tT})^*]$ induces the constructive interference, thus the bounds are also stronger. For the third (upper right) plot, both $[y_L^{tT}(y_R^{tT})^* + y_R^{tT}(y_L^{tT})^*]$ and $[y_L^{tT}(y_R^{tT})^* - y_R^{tT}(y_L^{tT})^*]$ vanish, thus it is less constrained compared to other plots. Besides, there can be more cancellation between the triangle and box diagrams for larger δ_{hh} . Thus the constraints are usually looser than the zero δ_{hh} ones.

In fact, we find that the di-Higgs production at HL-LHC can give stronger constraints than those from perturbative unitarity and $h \rightarrow \gamma Z$ decay. When we take into account the top quark EDM bound, the two scenarios $\text{Re}(y_L^{tT}) = \text{Im}(y_L^{tT}) = 0$ and $y_L^{tT} = (y_R^{tT})^*$ can also be constrained. For the other scenarios $y_R^{tT} = 0, y_L^{tT} = \pm y_R^{tT}, \text{Im}y_L^{tT} = \text{Im}y_R^{tT} = 0$, they are insensitive to the top quark EDM. Because we have the relation $d_t^{EDM} \sim y_R^{tT}(y_L^{tT})^* - y_L^{tT}(y_R^{tT})^* = 2i(\text{Re}y_L^{tT}\text{Im}y_R^{tT} - \text{Re}y_R^{tT}\text{Im}y_L^{tT})$. For the scenarios $\text{Re}(y_L^{tT}) = \text{Im}(y_R^{tT}) = 0$ and $y_L^{tT} = (y_R^{tT})^*$, we compare the bounds from di-Higgs production and top quark EDM for $\delta_{hh} = 0$ (Fig. 5) and $\delta_{hh} = 0.5$ (Fig. 6), respectively. From these plots, we can find that the off-axis regions can be strongly bounded by the top EDM, while it will lose the constraining power in the near axis regions.

V.2. The benchmark point $m_T = 800$ GeV and $s_L = 0.1$

For the case of $m_T = 800$ GeV and $s_L = 0.1$, the numerical results of μ_{hh} are evaluated as

$$\begin{aligned} \mu_{hh} = & 1 - 0.04939 - 0.7814 \delta_{hh} + 0.281 \delta_{hh}^2 + (0.1279 - 0.04494 \delta_{hh})(|y_L^{tT}|^2 + |y_R^{tT}|^2) \\ & + (1.087 - 0.5731 \delta_{hh})[y_L^{tT}(y_R^{tT})^* + y_R^{tT}(y_L^{tT})^*] + 0.01943(|y_L^{tT}|^2 + |y_R^{tT}|^2)^2 + 0.378[y_L^{tT}(y_R^{tT})^* + y_R^{tT}(y_L^{tT})^*]^2 \\ & + 0.0711(|y_L^{tT}|^2 + |y_R^{tT}|^2)[y_L^{tT}(y_R^{tT})^* + y_R^{tT}(y_L^{tT})^*] - 0.9907[y_L^{tT}(y_R^{tT})^* - y_R^{tT}(y_L^{tT})^*]^2. \end{aligned} \quad (27)$$

In this case, the present di-Higgs production experiments give the constraints $\delta_{hh} \in (-3.42, 6.20)$ and $\text{Re}y_L^{tT}, \text{Im}y_L^{tT}, \text{Re}y_R^{tT}, \text{Im}y_R^{tT} \in (-3.81, 3.81)$ at 95% CL by setting one parameter at a time. In Tab. V, we give the expected constraints on the parameters $\delta_{hh}, \text{Re}y_L^{tT}, \text{Im}y_L^{tT}, \text{Re}y_R^{tT}, \text{Im}y_R^{tT}$ at HL-LHC.

parameters		δ_{hh}	$\text{Re}y_L^{tT}$	$\text{Im}y_L^{tT}$	$\text{Re}y_R^{tT}$	$\text{Im}y_R^{tT}$
method	individual	(-0.499, 0.541) \cup (2.24, 3.28)	(-1.61, 1.61)	(-1.61, 1.61)	(-1.61, 1.61)	(-1.61, 1.61)
	2 σ	(-0.852, 3.63)	(-2.04, 2.04)	(-2.04, 2.04)	(-2.04, 2.04)	(-2.04, 2.04)
marginalized	1 σ	(-4.12, 3.89)	(-2.82, 2.82)	(-2.82, 2.82)	(-2.82, 2.82)	(-2.82, 2.82)
	2 σ	(-4.80, 4.51)	(-3.05, 3.05)	(-3.05, 3.05)	(-3.05, 3.05)	(-3.05, 3.05)

TABLE V. The expected 1σ and 2σ bounds at HL-LHC for the parameters $\delta_{hh}, \text{Re}y_L^{tT}, \text{Im}y_L^{tT}, \text{Re}y_R^{tT}, \text{Im}y_R^{tT}$ under the benchmark point $m_T = 800$ GeV and $s_L = 0.1$. Here we adopt two different methods: (1) turn on one parameter at a time, namely the individual method; (2) turn on all the five parameters, namely the marginalized method.

We will also plot the reached two-dimensional parameter space by setting two of them to be zero or imposing two conditions. In Fig. 7 and Fig. 8, similar plots are presented for the six scenarios

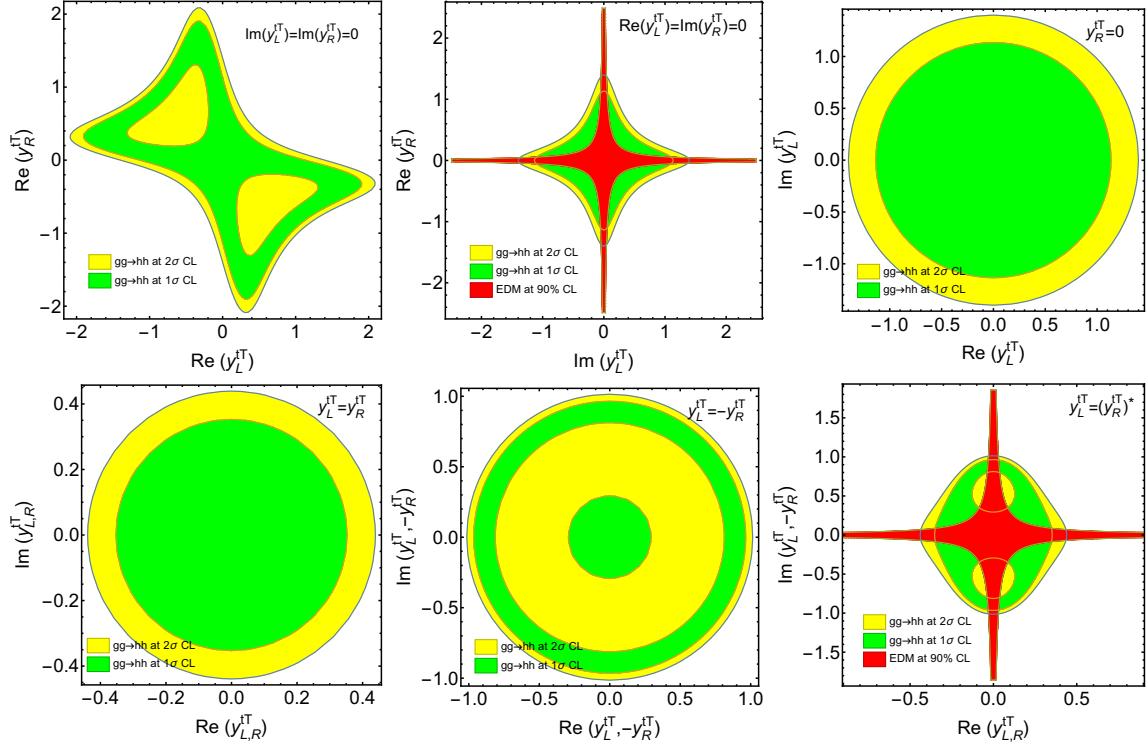


FIG. 5. The reach regions of y_L^{tT}, y_R^{tT} at HL-LHC with $\delta_{hhh} = 0$ for the case of $m_T = 400$ GeV and $s_L = 0.2$. In the above plots, we take $\text{Im}(y_L^{tT}) = \text{Im}(y_R^{tT}) = 0$ (upper left), $\text{Re}(y_L^{tT}) = \text{Im}(y_R^{tT}) = 0$ (upper central), $y_R^{tT} = 0$ (upper right), $y_L^{tT} = y_R^{tT}$ (lower left), $y_L^{tT} = -y_R^{tT}$ (lower central), and $y_L^{tT} = (y_R^{tT})^*$ (lower right) respectively. We also take into account the top quark EDM constraint for the scenarios $\text{Re}(y_L^{tT}) = \text{Im}(y_R^{tT}) = 0$ (upper central) and $y_L^{tT} = (y_R^{tT})^*$ (lower right), where the reach regions of y_L^{tT}, y_R^{tT} are shown in red at 90% CL.

with $\delta_{hhh} = 0$ and $\delta_{hhh} = 0.5$, respectively. From these plots, we find that $\text{Re}(y_{L,R}^{tT})$ and $\text{Im}(y_{L,R}^{tT})$ are constrained to be in the range $(-3, 3)$ roughly at 2σ CL. In some of these scenarios, the 2σ interval can be tight as $(-0.5, 0.5)$. The reach regions are similar to those in the $m_T = 400$ GeV and $s_L = 0.2$ case. For the scenarios $\text{Re}(y_L^{tT}) = \text{Im}(y_R^{tT}) = 0$ and $y_L^{tT} = (y_R^{tT})^*$, we also compare the bounds from di-Higgs production and top quark EDM for $\delta_{hhh} = 0$ (Fig. 7) and $\delta_{hhh} = 0.5$ (Fig. 8), respectively. When m_T becomes larger, $y_{L,R}^{tT}$ are constrained more loosely. When s_L becomes very small, the pure top quark contributions are SM-like and the pure T quark contributions are highly suppressed. Thus, the main deviation of μ_{hh} is from the FCNY interactions.

By the way, the FCNY coupling may be probed through other processes too. For example, we can probe the FCNY coupling Tth through direct production processes $pp \rightarrow T\bar{t}h, T\bar{t}, ThW, Thj$. But they suffer from low event rate, the detailed analyses in these channels are beyond the scope of this work.

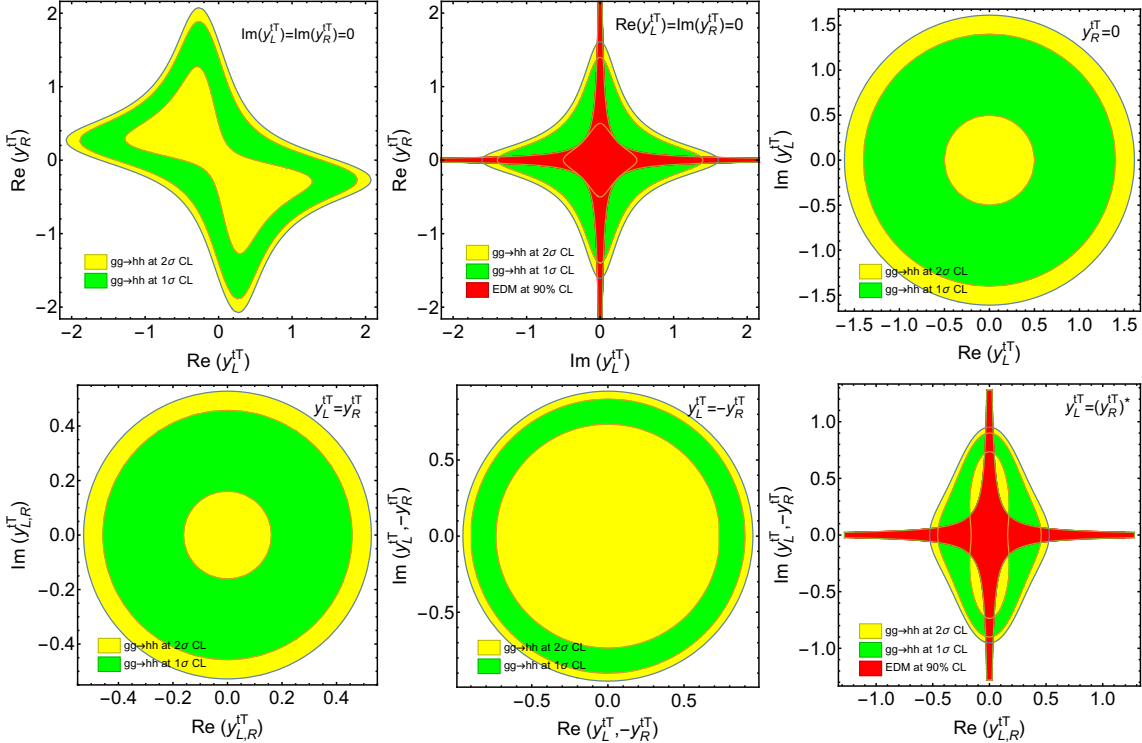


FIG. 6. The reach regions of y_L^{tT}, y_R^{tT} at HL-LHC with $\delta_{hhh} = 0.5$ for the case of $m_T = 400$ GeV and $s_L = 0.2$. In the above plots, we take $\text{Im}(y_L^{tT}) = \text{Im}(y_R^{tT}) = 0$ (upper left), $\text{Re}(y_L^{tT}) = \text{Im}(y_R^{tT}) = 0$ (upper central), $y_R^{tT} = 0$ (upper right), $y_L^{tT} = y_R^{tT}$ (lower left), $y_L^{tT} = -y_R^{tT}$ (lower central), and $y_L^{tT} = (y_R^{tT})^*$ (lower right) respectively. We also take into account the top quark EDM constraint for the scenarios $\text{Re}(y_L^{tT}) = \text{Im}(y_R^{tT}) = 0$ (upper central) and $y_L^{tT} = (y_R^{tT})^*$ (lower right), where the reach regions of y_L^{tT}, y_R^{tT} are shown in red at 90% CL.

V.3. Comments on the doublet and triplet vector-like quarks

We have assumed $T_{L,R}$ to be singlets throughout this work, while they can be components of the doublet or triplet VLQs. There are two doublet and two triplet VLQs containing the T quark: $(X, T)_{L,R}, (T, B)_{L,R}, (X, T, B)_{L,R}, (T, B, Y)_{L,R}$. Here X, B, Y carry $\frac{4}{3}, -\frac{1}{3}, -\frac{4}{3}$ electric charges, respectively. For the doublet $(X, T)_{L,R}$, the Higgs particle only interact with the $T_{L,R}$. For the doublet $(T, B)_{L,R}$ and triplets $(X, T, B)_{L,R}, (T, B, Y)_{L,R}$, the B quark can mix with the SM bottom quark. Thus, the Higgs particle will interact with both the T and B quarks. Let us denote left (right) up-type and down-type quark mixing angles as θ_L^t (θ_R^t) and θ_L^b (θ_R^b). They can be related with each other [6].

- For the triplet $(X, T, B)_{L,R}$, we have the relations $\tan \theta_R^t = \frac{m_t}{m_T} \tan \theta_L^t$ and $\tan \theta_R^b = \frac{m_b}{m_B} \tan \theta_L^b$. θ_L^t and θ_L^b can be related through the identity $\sin 2\theta_L^b = \sqrt{2} \frac{m_T^2 - m_b^2}{m_B^2 - m_b^2} \sin 2\theta_L^t$. Thus, there is only one independent mixing angle θ_L^t .

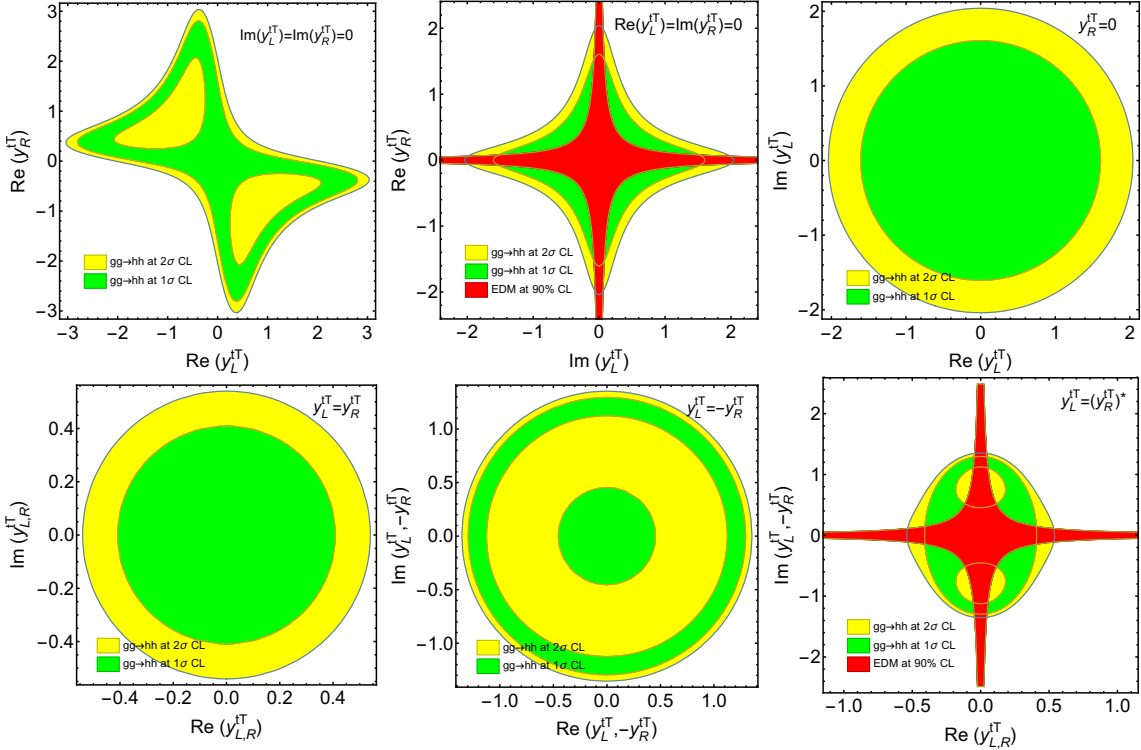


FIG. 7. The reach regions of y_L^{tT}, y_R^{tT} at HL-LHC with $\delta_{hhh} = 0$ for the case of $m_T = 800$ GeV and $s_L = 0.1$. In the above plots, we take $\text{Im}(y_L^{tT}) = \text{Im}(y_R^{tT}) = 0$ (upper left), $\text{Re}(y_L^{tT}) = \text{Im}(y_R^{tT}) = 0$ (upper central), $y_R^{tT} = 0$ (upper right), $y_L^{tT} = y_R^{tT}$ (lower left), $y_L^{tT} = -y_R^{tT}$ (lower central), and $y_L^{tT} = (y_R^{tT})^*$ (lower right) respectively. We also take into account the top quark EDM constraint for the scenarios $\text{Re}(y_L^{tT}) = \text{Im}(y_R^{tT}) = 0$ (upper central) and $y_L^{tT} = (y_R^{tT})^*$ (lower right), where the reach regions of y_L^{tT}, y_R^{tT} are shown in red at 90% CL.

- For the triplet $(T, B, Y)_{L,R}$, we have the relations $\tan \theta_R^t = \frac{m_t}{m_T} \tan \theta_L^t$ and $\tan \theta_R^b = \frac{m_b}{m_B} \tan \theta_L^b$. θ_L^t and θ_L^b can be related through the identity $\sin 2\theta_L^b = \frac{1}{\sqrt{2}} \frac{m_T^2 - m_t^2}{m_B^2 - m_b^2} \sin 2\theta_L^t$. Thus, there is only one independent mixing angle θ_L^t .
- For the doublet $(X, T)_{L,R}$, we have the relation $\tan \theta_L^t = \frac{m_t}{m_T} \tan \theta_R^t$. Thus, there is only one independent mixing angle θ_R^t .
- For the doublet $(T, B)_{L,R}$, we have the relations $\tan \theta_L^t = \frac{m_t}{m_T} \tan \theta_R^t$ and $\tan \theta_L^b = \frac{m_b}{m_B} \tan \theta_R^b$. Thus, there are two independent mixing angles θ_R^t and θ_R^b .

For the doublet $(X, T)_{L,R}$, the constraints on FCNY couplings from di-Higgs production are similar to those in the singlet $T_{L,R}$ case. Compared to the singlet $T_{L,R}$, there are extra BBh, Bbh type Yukawa interactions for the doublet $(T, B)_{L,R}$ and triplets $(X, T, B)_{L,R}, (T, B, Y)_{L,R}$. Thus, it is expected that the constraints on FCNY interactions are looser.

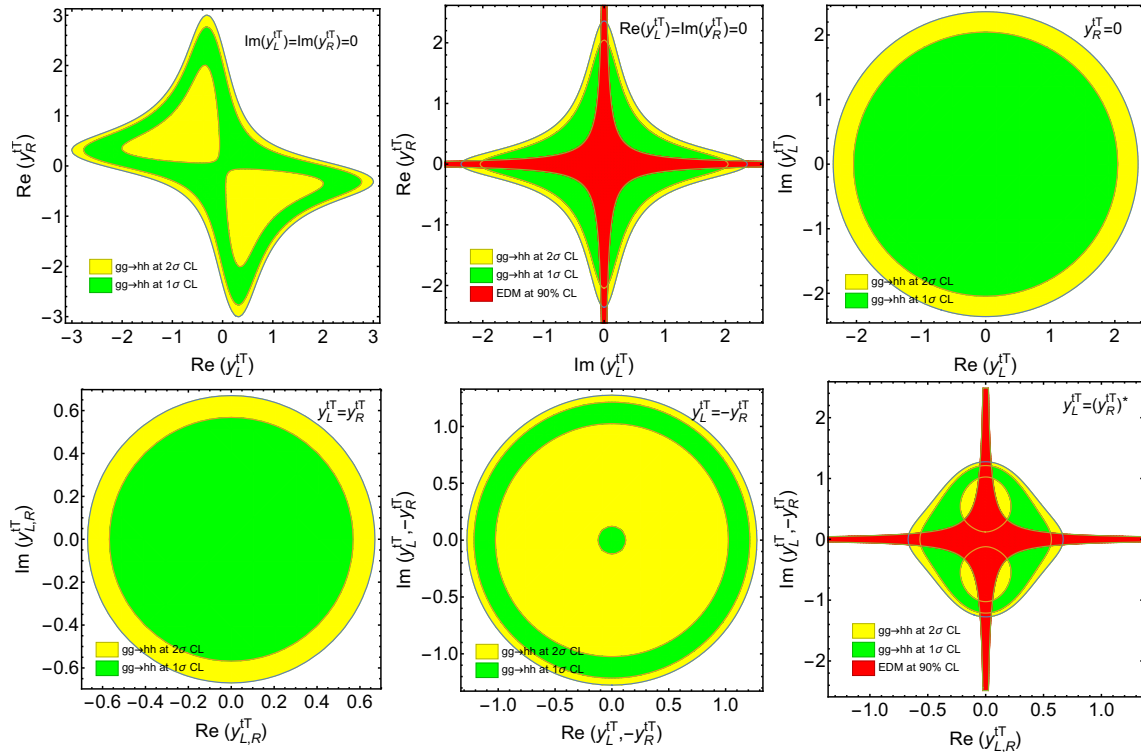


FIG. 8. The reach regions of y_L^{tT}, y_R^{tT} at HL-LHC with $\delta_{hhh} = 0.5$ for the case of $m_T = 800$ GeV and $s_L = 0.1$. In the above plots, we take $\text{Im}(y_L^{tT}) = \text{Im}(y_R^{tT}) = 0$ (upper left), $\text{Re}(y_L^{tT}) = \text{Im}(y_R^{tT}) = 0$ (upper central), $y_R^{tT} = 0$ (upper right), $y_L^{tT} = y_R^{tT}$ (lower left), $y_L^{tT} = -y_R^{tT}$ (lower central), and $y_L^{tT} = (y_R^{tT})^*$ (lower right) respectively. We also take into account the top quark EDM constraint for the scenarios $\text{Re}(y_L^{tT}) = \text{Im}(y_R^{tT}) = 0$ (upper central) and $y_L^{tT} = (y_R^{tT})^*$ (lower right), where the reach regions of y_L^{tT}, y_R^{tT} are shown in red at 90% CL.

VI. SUMMARY AND CONCLUSIONS

Top partners are well motivated in many new physics models and FCNY interactions can appear between top quark and the new heavy quark. To unveil the nature of flavor structure and EWSB, it is important to probe the FCNY interactions. However, it is challenging to constrain the $T\bar{t}h$ coupling at both current and future experiments directly.

In this paper, we have introduced a simplified model and summarized the main constraints from theoretical and experimental viewpoints first. Then we calculate the amplitude of di-Higgs production. After choosing $m_T = 400$ GeV, $s_L = 0.2$ and $m_T = 800$ GeV, $s_L = 0.1$ as benchmark points, we evaluate the numerical cross sections. It is found that the present constraints from di-Higgs production have already surpassed the unitarity bound because of the $(y_{L,R}^{tT})^4$ behavior in di-Higgs production cross section. For the case of $m_T = 400$ GeV and $s_L = 0.2$, $\text{Re}y_{L,R}^{tT}$ and $\text{Im}y_{L,R}^{tT}$ are expected to be bounded in the range $(-2, 2)$, and even $(-0.4, 0.4)$ in some scenarios at HL-LHC with 2σ CL roughly. For the case of $m_T = 800$ GeV and $s_L = 0.1$, $\text{Re}y_{L,R}^{tT}$ and $\text{Im}y_{L,R}^{tT}$ are expected

to be bounded in the range $(-3, 3)$, and even $(-0.5, 0.5)$ in some scenarios at HL-LHC with 2σ CL roughly. The value of δ_{hhh} can have significant effects on the constraints of $y_{L,R}^{tT}$. Simply speaking, larger δ_{hhh} leads to looser constraints on $y_{L,R}^{tT}$, because there can be more cancellation between the triangle and box diagrams. Finally, we find that the top quark EDM can give stronger bounds of $y_{L,R}^{tT}$ in the off-axis regions for some scenarios.

ACKNOWLEDGEMENTS

We would like to thank Gang Li, Zhao Li, Ying-nan Mao, and Hao Zhang for helpful discussions. We also thank Olivier Mattelaer for MadGraph program discussions through the launchpad platform.

- [1] S. L. Glashow. Partial Symmetries of Weak Interactions. *Nucl. Phys.*, 22:579–588, 1961.
- Steven Weinberg. A Model of Leptons. *Phys. Rev. Lett.*, 19:1264–1266, 1967.
- Abdus Salam. Weak and Electromagnetic Interactions. *Conf. Proc.*, C680519:367–377, 1968.
- [2] M. Tanabashi et al. Review of Particle Physics. *Phys. Rev.*, D98(3):030001, 2018.
- [3] F. Englert and R. Brout. Broken Symmetry and the Mass of Gauge Vector Mesons. *Phys. Rev. Lett.*, 13:321–323, 1964.
- Peter W. Higgs. Broken symmetries, massless particles and gauge fields. *Phys. Lett.*, 12:132–133, 1964.
- G. S. Guralnik, C. R. Hagen, and T. W. B. Kibble. Global Conservation Laws and Massless Particles. *Phys. Rev. Lett.*, 13:585–587, 1964.
- T. W. B. Kibble. Symmetry breaking in nonAbelian gauge theories. *Phys. Rev.*, 155:1554–1561, 1967.
- [4] Georges Aad et al. Observation of a new particle in the search for the Standard Model Higgs boson with the ATLAS detector at the LHC. *Phys. Lett.*, B716:1–29, 2012.
- Serguei Chatrchyan et al. Observation of a new boson at a mass of 125 GeV with the CMS experiment at the LHC. *Phys. Lett.*, B716:30–61, 2012.
- [5] J. A. Aguilar-Saavedra. Identifying top partners at LHC. *JHEP*, 11:030, 2009.
- [6] J. A. Aguilar-Saavedra, R. Benbrik, S. Heinemeyer, and M. Pérez-Victoria. Handbook of vectorlike quarks: Mixing and single production. *Phys. Rev.*, D88(9):094010, 2013.
- [7] S. Dittmaier et al. Handbook of LHC Higgs Cross Sections: 1. Inclusive Observables. 2011.
- S. Dittmaier et al. Handbook of LHC Higgs Cross Sections: 2. Differential Distributions. 2012.
- J R Andersen et al. Handbook of LHC Higgs Cross Sections: 3. Higgs Properties. 2013.
- D. de Florian et al. Handbook of LHC Higgs Cross Sections: 4. Deciphering the Nature of the Higgs Sector. 2016.
- [8] Shi-Ping He. Higgs boson to γZ decay as a probe of flavor-changing neutral Yukawa couplings. *Phys. Rev. D*, 102(7):075035, 2020.
- [9] S. Dawson and E. Furlan. A Higgs Conundrum with Vector Fermions. *Phys. Rev.*, D86:015021, 2012.
- [10] Andrea De Simone, Oleksii Matsedonskyi, Riccardo Rattazzi, and Andrea Wulzer. A First Top Partner Hunter’s Guide. *JHEP*, 04:004, 2013.
- [11] F. del Aguila, M. Perez-Victoria, and Jose Santiago. Effective description of quark mixing. *Phys. Lett.*, B492:98–106, 2000.
- [12] F. del Aguila, M. Perez-Victoria, and Jose Santiago. Observable contributions of new exotic quarks to quark mixing. *JHEP*, 09:011, 2000.
- [13] J. A. Aguilar-Saavedra. Effects of mixing with quark singlets. *Phys. Rev.*, D67:035003, 2003. [Erratum: *Phys. Rev.* D69, 099901(2004)].
- [14] Matthew J. Dolan, J. L. Hewett, M. Krämer, and T. G. Rizzo. Simplified Models for Higgs Physics: Singlet Scalar and Vector-like Quark Phenomenology. *JHEP*, 07:039, 2016.

- [15] Jeong Han Kim and Ian M. Lewis. Loop Induced Single Top Partner Production and Decay at the LHC. *JHEP*, 05:095, 2018.
- [16] J. A. Aguilar-Saavedra, D. E. López-Fogliani, and C. Muñoz. Novel signatures for vector-like quarks. *JHEP*, 06:095, 2017.
- [17] Margarete Mühlleitner, Marco O. P. Sampaio, Rui Santos, and Jonas Wittbrodt. The N2HDM under Theoretical and Experimental Scrutiny. *JHEP*, 03:094, 2017.
- [18] Kingman Cheung, Shi-Ping He, Ying-nan Mao, Po-Yan Tseng, and Chen Zhang. Phenomenology of a little Higgs pseudoaxion. *Phys. Rev.*, D98(7):075023, 2018.
- [19] Giacomo Cacciapaglia, Thomas Flacke, Myeonghun Park, and Mengchao Zhang. Exotic decays of top partners: mind the search gap. *Phys. Lett. B*, 798:135015, 2019.
- [20] Mathieu Buchkremer, Giacomo Cacciapaglia, Aldo Deandrea, and Luca Panizzi. Model Independent Framework for Searches of Top Partners. *Nucl. Phys.*, B876:376–417, 2013.
- [21] Shinya Kanemura, Yasuhiro Okada, Eibun Senaha, and C.-P. Yuan. Higgs coupling constants as a probe of new physics. *Phys. Rev. D*, 70:115002, 2004.
- [22] Shi-Ping He and Shou-hua Zhu. One-Loop Radiative Correction to the Triple Higgs Coupling in the Higgs Singlet Model. *Phys. Lett.*, B764:31–37, 2017.
- [23] Shinya Kanemura, Mariko Kikuchi, and Kei Yagyu. One-loop corrections to the Higgs self-couplings in the singlet extension. *Nucl. Phys.*, B917:154–177, 2017.
- [24] Abdesslam Arhrib, Rachid Benbrik, Jaouad El Falaki, and Adil Jueid. Radiative corrections to the Triple Higgs Coupling in the Inert Higgs Doublet Model. *JHEP*, 12:007, 2015.
- [25] Shinya Kanemura, Mariko Kikuchi, Kodai Sakurai, and Kei Yagyu. H-COUP: a program for one-loop corrected Higgs boson couplings in non-minimal Higgs sectors. *Comput. Phys. Commun.*, 233:134–144, 2018.
- [26] Cheng-Wei Chiang, An-Li Kuo, and Kei Yagyu. One-loop renormalized Higgs boson vertices in the Georgi-Machacek model. *Phys. Rev. D*, 98(1):013008, 2018.
- [27] Johannes Braathen and Shinya Kanemura. On two-loop corrections to the Higgs trilinear coupling in models with extended scalar sectors. *Phys. Lett. B*, 796:38–46, 2019.
- [28] Christoph Englert and Joerg Jaeckel. Probing the Symmetric Higgs Portal with Di-Higgs Boson Production. *Phys. Rev. D*, 100(9):095017, 2019.
- [29] Shinya Kanemura, Mariko Kikuchi, Kentarou Mawatari, Kodai Sakurai, and Kei Yagyu. H-COUP Version 2: a program for one-loop corrected Higgs boson decays in non-minimal Higgs sectors. *Comput. Phys. Commun.*, 257:107512, 2020.
- [30] Christoph Englert, Joerg Jaeckel, Michael Spannowsky, and Panagiotis Stylianou. Power meets Precision to explore the Symmetric Higgs Portal. *Phys. Lett. B*, 806:135526, 2020.
- [31] Michael E. Peskin and Tatsu Takeuchi. A New constraint on a strongly interacting Higgs sector. *Phys. Rev. Lett.*, 65:964–967, 1990.
- [32] Michael E. Peskin and Tatsu Takeuchi. Estimation of oblique electroweak corrections. *Phys. Rev.*, D46:381–409, 1992.
- [33] L.avoura and Joao P. Silva. The Oblique corrections from vector - like singlet and doublet quarks. *Phys. Rev.*, D47:2046–2057, 1993.
- [34] Chien-Yi Chen, S. Dawson, and Elisabetta Furlan. Vectorlike fermions and Higgs effective field theory revisited. *Phys. Rev.*, D96(1):015006, 2017.
- [35] Jacob Baron et al. Order of Magnitude Smaller Limit on the Electric Dipole Moment of the Electron. *Science*, 343:269–272, 2014.
- [36] V. Andreev et al. Improved limit on the electric dipole moment of the electron. *Nature*, 562(7727):355–360, 2018.
- [37] Jernej F. Kamenik, Michele Papucci, and Andreas Weiler. Constraining the dipole moments of the top quark. *Phys. Rev. D*, 85:071501, 2012. [Erratum: Phys.Rev.D 88, 039903 (2013)].
- [38] V. Cirigliano, W. Dekens, J. de Vries, and E. Mereghetti. Is there room for CP violation in the top-Higgs sector? *Phys. Rev. D*, 94(1):016002, 2016.
- [39] V. Cirigliano, W. Dekens, J. de Vries, and E. Mereghetti. Constraining the top-Higgs sector of the Standard Model Effective Field Theory. *Phys. Rev. D*, 94(3):034031, 2016.

- [40] E.W.Nigel Glover and J.J. van der Bij. HIGGS BOSON PAIR PRODUCTION VIA GLUON FUSION. *Nucl. Phys. B*, 309:282–294, 1988.
- [41] Abdelhak Djouadi. The Anatomy of electro-weak symmetry breaking. I: The Higgs boson in the standard model. *Phys. Rept.*, 457:1–216, 2008.
- [42] Eri Asakawa, Daisuke Harada, Shinya Kanemura, Yasuhiro Okada, and Koji Tsumura. Higgs boson pair production in new physics models at hadron, lepton, and photon colliders. *Phys. Rev. D*, 82:115002, 2010.
- [43] Matthew J. Dolan, Christoph Englert, and Michael Spannowsky. New Physics in LHC Higgs boson pair production. *Phys. Rev. D*, 87(5):055002, 2013.
- [44] S. Dawson, A. Ismail, and Ian Low. What’s in the loop? The anatomy of double Higgs production. *Phys. Rev. D*, 91(11):115008, 2015.
- [45] Hong-Jian He, Jing Ren, and Weiming Yao. Probing new physics of cubic Higgs boson interaction via Higgs pair production at hadron colliders. *Phys. Rev. D*, 93(1):015003, 2016.
- [46] J. Alison et al. Higgs Boson Pair Production at Colliders: Status and Perspectives. In B. Di Micco, M. Gouzevitch, J. Mazzitelli, and C. Vernieri, editors, *Double Higgs Production at Colliders*, 9 2019.
- [47] Florian Goertz, Andreas Papaefstathiou, Li Lin Yang, and José Zurita. Higgs boson pair production in the D=6 extension of the SM. *JHEP*, 04:167, 2015.
- [48] Aleksandr Azatov, Roberto Contino, Giuliano Panico, and Minho Son. Effective field theory analysis of double Higgs boson production via gluon fusion. *Phys. Rev. D*, 92(3):035001, 2015.
- [49] Chih-Ting Lu, Jung Chang, Kingman Cheung, and Jae Sik Lee. An exploratory study of Higgs-boson pair production. *JHEP*, 08:133, 2015.
- [50] Qing-Hong Cao, Bin Yan, Dong-Ming Zhang, and Hao Zhang. Resolving the Degeneracy in Single Higgs Production with Higgs Pair Production. *Phys. Lett. B*, 752:285–290, 2016.
- [51] Qing-Hong Cao, Gang Li, Bin Yan, Dong-Ming Zhang, and Hao Zhang. Double Higgs production at the 14 TeV LHC and a 100 TeV pp collider. *Phys. Rev. D*, 96(9):095031, 2017.
- [52] Gang Li, Ling-Xiao Xu, Bin Yan, and C.-P. Yuan. Resolving the degeneracy in top quark Yukawa coupling with Higgs pair production. *Phys. Lett. B*, 800:135070, 2020.
- [53] Roberto Contino, Christophe Grojean, Mauro Moretti, Fulvio Piccinini, and Riccardo Rattazzi. Strong Double Higgs Production at the LHC. *JHEP*, 05:089, 2010.
- [54] Roberto Contino, Margherita Ghezzi, Mauro Moretti, Giuliano Panico, Fulvio Piccinini, and Andrea Wulzer. Anomalous Couplings in Double Higgs Production. *JHEP*, 08:154, 2012.
- [55] R. Grober, M. Muhlleitner, and M. Spira. Higgs Pair Production at NLO QCD for CP-violating Higgs Sectors. *Nucl. Phys. B*, 925:1–27, 2017.
- [56] G. Buchalla, M. Capozzi, A. Celis, G. Heinrich, and L. Scyboz. Higgs boson pair production in non-linear Effective Field Theory with full m_t -dependence at NLO QCD. *JHEP*, 09:057, 2018.
- [57] Chien-Yi Chen, S. Dawson, and I.M. Lewis. Exploring resonant di-Higgs boson production in the Higgs singlet model. *Phys. Rev. D*, 91(3):035015, 2015.
- [58] S. Dawson and I.M. Lewis. NLO corrections to double Higgs boson production in the Higgs singlet model. *Phys. Rev. D*, 92(9):094023, 2015.
- [59] Ian M. Lewis and Matthew Sullivan. Benchmarks for Double Higgs Production in the Singlet Extended Standard Model at the LHC. *Phys. Rev. D*, 96(3):035037, 2017.
- [60] Lan-Chun Lü, Chun Du, Yaquan Fang, Hong-Jian He, and Huijun Zhang. Searching heavier Higgs boson via di-Higgs production at LHC Run-2. *Phys. Lett. B*, 755:509–522, 2016.
- [61] Stefania De Curtis, Stefano Moretti, Kei Yagyu, and Emine Yildirim. Single and double SM-like Higgs boson production at future electron-positron colliders in composite 2HDMs. *Phys. Rev. D*, 95(9):095026, 2017.
- [62] Tadashi Kon, Takuto Nagura, Takahiro Ueda, and Kei Yagyu. Double Higgs boson production at e^+e^- colliders in the two-Higgs-doublet model. *Phys. Rev. D*, 99(9):095027, 2019.
- [63] Jing Ren, Rui-Qing Xiao, Maosen Zhou, Yaquan Fang, Hong-Jian He, and Weiming Yao. LHC Search of New Higgs Boson via Resonant Di-Higgs Production with Decays into 4W. *JHEP*, 06:090, 2018.
- [64] Sally Dawson, Elisabetta Furlan, and Ian Lewis. Unravelling an extended quark sector through multiple Higgs production? *Phys. Rev. D*, 87(1):014007, 2013.

- [65] Giacomo Cacciapaglia, Haiying Cai, Alexandra Carvalho, Aldo Deandrea, Thomas Flacke, Benjamin Fuks, Devdatta Majumder, and Hua-Sheng Shao. Probing vector-like quark models with Higgs-boson pair production. *JHEP*, 07:005, 2017.
- [66] Kingman Cheung, Adil Jueid, Chih-Ting Lu, Jeonghyeon Song, and Yeo Woong Yoon. Disentangling new physics effects on non-resonant Higgs boson pair production from gluon fusion. 3 2020.
- [67] M. Gillioz, R. Grober, C. Grojean, M. Mühlleitner, and E. Salvioni. Higgs Low-Energy Theorem (and its corrections) in Composite Models. *JHEP*, 10:004, 2012.
- [68] Ramona Grober, Margarete Mühlleitner, and Michael Spira. Signs of Composite Higgs Pair Production at Next-to-Leading Order. *JHEP*, 06:080, 2016.
- [69] T. Plehn, M. Spira, and P.M. Zerwas. Pair production of neutral Higgs particles in gluon-gluon collisions. *Nucl. Phys. B*, 479:46–64, 1996. [Erratum: Nucl.Phys.B 531, 655–655 (1998)].
- [70] S. Dawson, S. Dittmaier, and M. Spira. Neutral Higgs boson pair production at hadron colliders: QCD corrections. *Phys. Rev. D*, 58:115012, 1998.
- [71] Abdelhak Djouadi. The Anatomy of electro-weak symmetry breaking. II. The Higgs bosons in the minimal supersymmetric model. *Phys. Rept.*, 459:1–241, 2008.
- [72] Junjie Cao, Zhaoxia Heng, Liangliang Shang, Peihua Wan, and Jin Min Yang. Pair Production of a 125 GeV Higgs Boson in MSSM and NMSSM at the LHC. *JHEP*, 04:134, 2013.
- [73] Philipp Basler, Sally Dawson, Christoph Englert, and Margarete Mühlleitner. Showcasing HH production: Benchmarks for the LHC and HL-LHC. *Phys. Rev. D*, 99(5):055048, 2019.
- [74] D. Binosi, J. Collins, C. Kaufhold, and L. Theussl. JaxoDraw: A Graphical user interface for drawing Feynman diagrams. Version 2.0 release notes. *Comput. Phys. Commun.*, 180:1709–1715, 2009.
- [75] R. Mertig, M. Bohm, and Ansgar Denner. FEYN CALC: Computer algebraic calculation of Feynman amplitudes. *Comput. Phys. Commun.*, 64:345–359, 1991.
- [76] Vladyslav Shtabovenko, Rolf Mertig, and Frederik Orellana. New Developments in FeynCalc 9.0. *Comput. Phys. Commun.*, 207:432–444, 2016.
- [77] Ding Yu Shao, Chong Sheng Li, Hai Tao Li, and Jian Wang. Threshold resummation effects in Higgs boson pair production at the LHC. *JHEP*, 07:169, 2013.
- [78] Daniel de Florian and Javier Mazzitelli. Higgs Boson Pair Production at Next-to-Next-to-Leading Order in QCD. *Phys. Rev. Lett.*, 111:201801, 2013.
- [79] Daniel de Florian and Javier Mazzitelli. Higgs pair production at next-to-next-to-leading logarithmic accuracy at the LHC. *JHEP*, 09:053, 2015.
- [80] Giuseppe Degrassi, Pier Paolo Giardino, and Ramona Gröber. On the two-loop virtual QCD corrections to Higgs boson pair production in the Standard Model. *Eur. Phys. J. C*, 76(7):411, 2016.
- [81] S. Borowka, N. Greiner, G. Heinrich, S.P. Jones, M. Kerner, J. Schlenk, U. Schubert, and T. Zirke. Higgs Boson Pair Production in Gluon Fusion at Next-to-Leading Order with Full Top-Quark Mass Dependence. *Phys. Rev. Lett.*, 117(1):012001, 2016. [Erratum: Phys.Rev.Lett. 117, 079901 (2016)].
- [82] Massimiliano Grazzini, Gudrun Heinrich, Stephen Jones, Stefan Kallweit, Matthias Kerner, Jonas M. Lindert, and Javier Mazzitelli. Higgs boson pair production at NNLO with top quark mass effects. *JHEP*, 05:059, 2018.
- [83] Julien Baglio, Francisco Campanario, Seraina Glaus, Margarete Mühlleitner, Michael Spira, and Juraj Streicher. Gluon fusion into Higgs pairs at NLO QCD and the top mass scheme. *Eur. Phys. J. C*, 79(6):459, 2019.
- [84] Long-Bin Chen, Hai Tao Li, Hua-Sheng Shao, and Jian Wang. Higgs boson pair production via gluon fusion at N³LO in QCD. *Phys. Lett. B*, 803:135292, 2020.
- [85] Long-Bin Chen, Hai Tao Li, Hua-Sheng Shao, and Jian Wang. The gluon-fusion production of Higgs boson pair: N³LO QCD corrections and top-quark mass effects. *JHEP*, 03:072, 2020.
- [86] Alexandra Carvalho, Martino Dall’Osso, Tommaso Dorigo, Florian Goertz, Carlo A. Gottardo, and Mia Tosi. Higgs Pair Production: Choosing Benchmarks With Cluster Analysis. *JHEP*, 04:126, 2016.
- [87] Alexandra Carvalho, Martino Dall’Osso, Pablo De Castro Manzano, Tommaso Dorigo, Florian Goertz, Maxime Gouzevich, and Mia Tosi. Analytical parametrization and shape classification of anomalous HH production in the EFT approach. 7 2016.
- [88] Adam Alloul, Neil D. Christensen, Céline Degrande, Claude Duhr, and Benjamin Fuks. FeynRules 2.0 - A complete toolbox for tree-level phenomenology. *Comput. Phys. Commun.*, 185:2250–2300, 2014.

- [89] Celine Degrande, Claude Duhr, Benjamin Fuks, David Grellscheid, Olivier Mattelaer, and Thomas Reiter. UFO - The Universal FeynRules Output. *Comput. Phys. Commun.*, 183:1201–1214, 2012.
- [90] Thomas Hahn. Generating Feynman diagrams and amplitudes with FeynArts 3. *Comput. Phys. Commun.*, 140:418–431, 2001.
- [91] Celine Degrande. Automatic evaluation of UV and R2 terms for beyond the Standard Model Lagrangians: a proof-of-principle. *Comput. Phys. Commun.*, 197:239–262, 2015.
- [92] J. Alwall, R. Frederix, S. Frixione, V. Hirschi, F. Maltoni, O. Mattelaer, H. S. Shao, T. Stelzer, P. Torrielli, and M. Zaro. The automated computation of tree-level and next-to-leading order differential cross sections, and their matching to parton shower simulations. *JHEP*, 07:079, 2014.
- [93] Valentin Hirschi and Olivier Mattelaer. Automated event generation for loop-induced processes. *JHEP*, 10:146, 2015.
- [94] Albert M Sirunyan et al. Combination of searches for Higgs boson pair production in proton-proton collisions at $\sqrt{s} = 13$ TeV. *Phys. Rev. Lett.*, 122(12):121803, 2019.
- [95] Georges Aad et al. Combination of searches for Higgs boson pairs in pp collisions at $\sqrt{s} = 13$ TeV with the ATLAS detector. *Phys. Lett. B*, 800:135103, 2020.
- [96] M. Cepeda et al. *Report from Working Group 2: Higgs Physics at the HL-LHC and HE-LHC*, volume 7, pages 221–584. 12 2019.
- [97] T. Hahn and M. Perez-Victoria. Automatized one loop calculations in four-dimensions and D-dimensions. *Comput. Phys. Commun.*, 118:153–165, 1999.

APPENDIX

A. ASYMPTOTIC BEHAVIORS OF THE LOOP FUNCTIONS

A.1. The shorthand notations of C_0 and D_0 functions

The definitions of C_0 and D_0 function related with pure top quark loops are given as

$$\begin{aligned}
 C_0^t(\hat{s}) &\equiv C_0(0, 0, \hat{s}, m_t^2, m_t^2, m_t^2), \\
 C_0^t(m_h^2) &\equiv C_0(m_h^2, m_h^2, \hat{s}, m_t^2, m_t^2, m_t^2), \\
 C_0^t(\hat{t}) &\equiv C_0(0, m_h^2, \hat{t}, m_t^2, m_t^2, m_t^2), \\
 C_0^t(\hat{u}) &\equiv C_0(0, m_h^2, \hat{u}, m_t^2, m_t^2, m_t^2), \\
 D_0^t(\hat{t}, \hat{s}) &\equiv D_0(m_h^2, 0, 0, m_h^2, \hat{t}, \hat{s}, m_t^2, m_t^2, m_t^2, m_t^2), \\
 D_0^t(\hat{u}, \hat{s}) &\equiv D_0(m_h^2, 0, 0, m_h^2, \hat{u}, \hat{s}, m_t^2, m_t^2, m_t^2, m_t^2), \\
 D_0^t(\hat{t}, \hat{u}) &\equiv D_0(m_h^2, 0, m_h^2, 0, \hat{t}, \hat{u}, m_t^2, m_t^2, m_t^2, m_t^2). \tag{28}
 \end{aligned}$$

The definitions of C_0 and D_0 function related with pure T quark loops are given as

$$\begin{aligned}
 C_0^T(\hat{s}) &\equiv C_0(0, 0, \hat{s}, m_T^2, m_T^2, m_T^2), \\
 C_0^T(m_h^2) &\equiv C_0(m_h^2, m_h^2, \hat{s}, m_T^2, m_T^2, m_T^2), \\
 C_0^T(\hat{t}) &\equiv C_0(0, m_h^2, \hat{t}, m_T^2, m_T^2, m_T^2), \\
 C_0^T(\hat{u}) &\equiv C_0(0, m_h^2, \hat{u}, m_T^2, m_T^2, m_T^2), \\
 D_0^T(\hat{t}, \hat{s}) &\equiv D_0(m_h^2, 0, 0, m_h^2, \hat{t}, \hat{s}, m_T^2, m_T^2, m_T^2, m_T^2), \\
 D_0^T(\hat{u}, \hat{s}) &\equiv D_0(m_h^2, 0, 0, m_h^2, \hat{u}, \hat{s}, m_T^2, m_T^2, m_T^2, m_T^2), \\
 D_0^T(\hat{t}, \hat{u}) &\equiv D_0(m_h^2, 0, m_h^2, 0, \hat{t}, \hat{u}, m_T^2, m_T^2, m_T^2, m_T^2). \tag{29}
 \end{aligned}$$

The definitions of C_0 and D_0 function related with mixed t and T quark loops are given as

$$\begin{aligned} C_0^{tT}(m_h^2) &\equiv C_0(m_h^2, m_h^2, \hat{s}, m_t^2, m_T^2, m_t^2), \\ C_0^{tT}(\hat{t}) &\equiv C_0(0, m_h^2, \hat{t}, m_t^2, m_T^2, m_t^2), \\ C_0^{tT}(\hat{u}) &\equiv C_0(0, m_h^2, \hat{u}, m_t^2, m_T^2, m_t^2), \\ D_0^{tT}(\hat{t}, \hat{s}) &\equiv D_0(m_h^2, 0, 0, m_h^2, \hat{t}, \hat{s}, m_T^2, m_t^2, m_t^2, m_t^2), \\ D_0^{tT}(\hat{u}, \hat{s}) &\equiv D_0(m_h^2, 0, 0, m_h^2, \hat{u}, \hat{s}, m_T^2, m_t^2, m_t^2, m_t^2), \\ D_0^{tT}(\hat{t}, \hat{u}) &\equiv D_0(m_h^2, 0, m_h^2, 0, \hat{t}, \hat{u}, m_t^2, m_T^2, m_t^2, m_t^2), \end{aligned} \quad (30)$$

and

$$\begin{aligned} C_0^{Tt}(m_h^2) &\equiv C_0(m_h^2, m_h^2, \hat{s}, m_T^2, m_t^2, m_T^2), \\ C_0^{Tt}(\hat{t}) &\equiv C_0(0, m_h^2, \hat{t}, m_T^2, m_T^2, m_t^2), \\ C_0^{Tt}(\hat{u}) &\equiv C_0(0, m_h^2, \hat{u}, m_T^2, m_T^2, m_t^2), \\ D_0^{Tt}(\hat{t}, \hat{s}) &\equiv D_0(m_h^2, 0, 0, m_h^2, \hat{t}, \hat{s}, m_t^2, m_T^2, m_T^2, m_T^2), \\ D_0^{Tt}(\hat{u}, \hat{s}) &\equiv D_0(m_h^2, 0, 0, m_h^2, \hat{u}, \hat{s}, m_t^2, m_T^2, m_T^2, m_T^2), \\ D_0^{Tt}(\hat{t}, \hat{u}) &\equiv D_0(m_h^2, 0, m_h^2, 0, \hat{t}, \hat{u}, m_T^2, m_t^2, m_t^2, m_T^2). \end{aligned} \quad (31)$$

As a matter of fact, we have the relation $D_0^{tT}(\hat{t}, \hat{u}) = D_0^{Tt}(\hat{t}, \hat{u})$.

A.2. Heavy quark expansion of C_0 function

C_0 function is defined as

$$\begin{aligned} &C_0(k_1^2, k_{12}^2, k_2^2, m_0^2, m_1^2, m_2^2) \\ &\equiv \frac{(2\pi\mu)^{4-D}}{i\pi^2} \int d^D q \frac{1}{(q^2 - m_0^2)[(q + k_1)^2 - m_1^2][(q + k_2)^2 - m_2^2]} \\ &= - \int_0^1 \int_0^1 \int_0^1 dx dy dz \frac{\delta(x + y + z - 1)}{xm_0^2 + ym_1^2 + zm_2^2 - xyk_1^2 - xzk_2^2 - yzk_{12}^2}, \end{aligned} \quad (32)$$

where $k_{12} \equiv k_1 - k_2$ and D is the dimension of space time. When the three internal masses are all equal, C_0 function can be expanded as [77]

$$\begin{aligned} &C_0(k_1^2, k_{12}^2, k_2^2, m_t^2, m_t^2, m_t^2) \\ &= - \int_0^1 \int_0^1 \int_0^1 dx dy dz \frac{\delta(x + y + z - 1)}{m_t^2 - xyk_1^2 - xzk_2^2 - yzk_{12}^2} \\ &= - \frac{1}{2m_t^2} - \frac{k_1^2 + k_2^2 + k_{12}^2}{24m_t^4} - \frac{k_1^4 + k_2^4 + k_{12}^4 + k_1^2k_2^2 + k_1^2k_{12}^2 + k_2^2k_{12}^2}{180m_t^6} + \mathcal{O}\left(\frac{k^6}{m_t^8}\right). \end{aligned} \quad (33)$$

Especially, we have the following results:

$$\begin{aligned} C_0^t(\hat{s}) &\approx -\frac{1}{2m_t^2}(1 + \frac{\hat{s}}{12m_t^2} + \frac{\hat{s}^2}{90m_t^4}), \\ C_0^t(m_h^2) &\approx -\frac{1}{2m_t^2}(1 + \frac{2m_h^2 + \hat{s}}{12m_t^2} + \frac{3m_h^4 + 2m_h^2\hat{s} + \hat{s}^2}{90m_t^4}), \\ C_0^t(\hat{t}) &\approx -\frac{1}{2m_t^2}(1 + \frac{m_h^2 + \hat{t}}{12m_t^2} + \frac{m_h^4 + m_h^2\hat{t} + \hat{t}^2}{90m_t^4}). \end{aligned} \quad (34)$$

The expansion of $C_0^t(\hat{u})$ functions can be obtained when replacing the \hat{t} in $C_0^t(\hat{t})$ by \hat{u} . The expansion of C_0^T functions can be obtained when replacing the m_t in C_0^t by m_T .

When the first two internal masses are equal, C_0 function can be expanded as

$$\begin{aligned} &C_0(k_1^2, k_{12}^2, k_2^2, m_t^2, m_t^2, m_T^2) \\ &= -\int_0^1 \int_0^1 \int_0^1 dx dy dz \frac{\delta(x+y+z-1)}{(x+y)m_t^2 + zm_T^2 - xyk_1^2 - xzk_2^2 - yzk_{12}^2} \\ &= -\int_0^1 \int_0^1 \int_0^1 dx dy dz \frac{\delta(x+y+z-1)}{(x+y)m_t^2 + zm_T^2} [1 + \frac{xyk_1^2 + xzk_2^2 + yzk_{12}^2}{(x+y)m_t^2 + zm_T^2} + \frac{(xyk_1^2 + xzk_2^2 + yzk_{12}^2)^2}{((x+y)m_t^2 + zm_T^2)^2}] + \mathcal{O}(\frac{k^6}{m_{t,T}^8}) \\ &\approx \frac{1 + \log r_{tT}^2 - r_{tT}^2}{m_T^2(1 - r_{tT}^2)^2} - \frac{2 + 6r_{tT}^2 \log r_{tT}^2 + 3r_{tT}^2 - 6r_{tT}^4 + r_{tT}^6}{12m_T^4 r_{tT}^2 (1 - r_{tT}^2)^4} k_1^2 \\ &\quad + \frac{5 + 2(1 + 2r_{tT}^2) \log r_{tT}^2 - 4r_{tT}^2 - r_{tT}^4}{4m_T^4 (1 - r_{tT}^2)^4} (k_2^2 + k_{12}^2) \\ &\quad - \frac{3 - 30r_{tT}^2 - 20r_{tT}^4 (1 + 3 \log r_{tT}^2) + 60r_{tT}^6 - 15r_{tT}^8 + 2r_{tT}^{10}}{180m_T^6 r_{tT}^4 (1 - r_{tT}^2)^6} k_1^4 \\ &\quad + \frac{10 + 9r_{tT}^2 + 3(1 + 6r_{tT}^2 + 3r_{tT}^4) \log r_{tT}^2 - 18r_{tT}^4 - r_{tT}^6}{9m_T^6 (1 - r_{tT}^2)^6} (k_{12}^4 + k_2^2 k_{12}^2 + k_2^4) \\ &\quad - \frac{3 + 44r_{tT}^2 + 12r_{tT}^4 (2 + 3r_{tT}^2) \log r_{tT}^2 - 36r_{tT}^4 - 12r_{tT}^6 + r_{tT}^8}{36m_T^6 r_{tT}^2 (1 - r_{tT}^2)^6} k_1^2 (k_2^2 + k_{12}^2). \end{aligned} \quad (35)$$

When the first and third internal masses are equal, C_0 function can be correlated with the first two mass equal cases through the following relations

$$\begin{aligned} C_0(k_1^2, k_{12}^2, k_2^2, m_t^2, m_T^2, m_t^2) &= C_0(k_2^2, k_{12}^2, k_1^2, m_t^2, m_t^2, m_T^2), \\ C_0(k_1^2, k_{12}^2, k_2^2, m_T^2, m_t^2, m_T^2) &= C_0(k_2^2, k_{12}^2, k_1^2, m_T^2, m_T^2, m_t^2). \end{aligned} \quad (36)$$

Especially, we have the following results

$$\begin{aligned}
C_0^{tT}(\hat{t}) &\approx \frac{1}{m_T^2} \cdot \frac{1 + \log r_{tT}^2 - r_{tT}^2}{(1 - r_{tT}^2)^2} + \frac{m_h^2 + \hat{t}}{m_T^4} \cdot \frac{5 + 2(1 + 2r_{tT}^2) \log r_{tT}^2 - 4r_{tT}^2 - r_{tT}^4}{4(1 - r_{tT}^2)^4} \\
&+ \frac{m_h^4 + m_h^2 \hat{t} + \hat{t}^2}{m_T^6} \cdot \frac{10 + 3(1 + 6r_{tT}^2 + 3r_{tT}^4) \log r_{tT}^2 + 9r_{tT}^2 - 18r_{tT}^4 - r_{tT}^6}{9(1 - r_{tT}^2)^6}, \\
C_0^{tT}(m_h^2) &\approx \frac{1}{m_T^2} \cdot \frac{1 + \log r_{tT}^2 - r_{tT}^2}{(1 - r_{tT}^2)^2} - \frac{\hat{s}}{m_T^4} \cdot \frac{2 + 6r_{tT}^2 \log r_{tT}^2 + 3r_{tT}^2 - 6r_{tT}^4 + r_{tT}^6}{12r_{tT}^2(1 - r_{tT}^2)^4} \\
&+ \frac{m_h^2}{m_T^4} \cdot \frac{5 + 2(1 + 2r_{tT}^2) \log r_{tT}^2 - 4r_{tT}^2 - r_{tT}^4}{2(1 - r_{tT}^2)^4} + \frac{m_h^4}{m_T^6} \cdot \frac{10 + 3(1 + 6r_{tT}^2 + 3r_{tT}^4) \log r_{tT}^2 + 9r_{tT}^2 - 18r_{tT}^4 - r_{tT}^6}{3(1 - r_{tT}^2)^6} \\
&- \frac{m_h^2 \hat{s}}{m_T^6} \cdot \frac{3 + 12r_{tT}^2(2 + 3r_{tT}^2) \log r_{tT}^2 + 44r_{tT}^2 - 36r_{tT}^4 - 12r_{tT}^6 + r_{tT}^8}{18r_{tT}^2(1 - r_{tT}^2)^6} \\
&- \frac{\hat{s}^2}{m_T^6} \cdot \frac{3 - 30r_{tT}^2 - 60r_{tT}^4 \log r_{tT}^2 - 20r_{tT}^4 + 60r_{tT}^6 - 15r_{tT}^8 + 2r_{tT}^{10}}{180r_{tT}^4(1 - r_{tT}^2)^6}. \tag{37}
\end{aligned}$$

Keeping the terms up to $\mathcal{O}(\frac{1}{m_T^4})$ and considering the $\log r_{tT}^2$ enhanced terms, they can be simplified as

$$\begin{aligned}
C_0^{tT}(\hat{t}) &\approx \frac{1}{m_T^2} [1 + \log r_{tT}^2 + r_{tT}^2(1 + 2 \log r_{tT}^2) + \frac{m_h^2 + \hat{t}}{4m_T^2} (5 + 2 \log r_{tT}^2)], \\
C_0^{tT}(m_h^2) &\approx \frac{1}{m_T^2} [1 + \log r_{tT}^2 + r_{tT}^2(1 + 2 \log r_{tT}^2) - \frac{\hat{s}}{12m_T^2} (\frac{2}{r_{tT}^2} + 11 + 6 \log r_{tT}^2) + \frac{m_h^2}{2m_T^2} (5 + 2 \log r_{tT}^2)]. \tag{38}
\end{aligned}$$

Similarly, we can get the following results

$$\begin{aligned}
C_0^{Tt}(\hat{t}) &\approx -\frac{1}{m_T^2} \cdot \frac{1 + r_{tT}^2 \log r_{tT}^2 - r_{tT}^2}{(1 - r_{tT}^2)^2} - \frac{m_h^2 + \hat{t}}{m_T^4} \cdot \frac{1 + 2r_{tT}^2(2 + r_{tT}^2) \log r_{tT}^2 + 4r_{tT}^2 - 5r_{tT}^4}{4(1 - r_{tT}^2)^4} \\
&- \frac{m_h^4 + m_h^2 \hat{t} + \hat{t}^2}{m_T^6} \cdot \frac{1 + 3r_{tT}^2(3 + 6r_{tT}^2 + r_{tT}^4) \log r_{tT}^2 + 18r_{tT}^2 - 9r_{tT}^4 - 10r_{tT}^6}{9(1 - r_{tT}^2)^6}, \\
C_0^{Tt}(m_h^2) &\approx -\frac{1}{m_T^2} \cdot \frac{1 + r_{tT}^2 \log r_{tT}^2 - r_{tT}^2}{(1 - r_{tT}^2)^2} - \frac{\hat{s}}{m_T^4} \cdot \frac{1 - 6r_{tT}^2 - 6r_{tT}^4 \log r_{tT}^2 + 3r_{tT}^4 + 2r_{tT}^6}{12(1 - r_{tT}^2)^4} \\
&- \frac{m_h^2}{2m_T^4} \cdot \frac{1 + 2r_{tT}^2(2 + r_{tT}^2) \log r_{tT}^2 + 4r_{tT}^2 - 5r_{tT}^4}{(1 - r_{tT}^2)^4} - \frac{m_h^4}{m_T^6} \cdot \frac{1 + 3r_{tT}^2(3 + 6r_{tT}^2 + r_{tT}^4) \log r_{tT}^2 + 18r_{tT}^2 - 9r_{tT}^4 - 10r_{tT}^6}{3(1 - r_{tT}^2)^6} \\
&- \frac{m_h^2 \hat{s}}{m_T^6} \cdot \frac{1 - 12r_{tT}^2 - 12r_{tT}^4(3 + 2r_{tT}^2) \log r_{tT}^2 - 36r_{tT}^4 + 44r_{tT}^6 + 3r_{tT}^8}{18(1 - r_{tT}^2)^6} \\
&- \frac{\hat{s}^2}{m_T^6} \cdot \frac{2 - 15r_{tT}^2 + 60r_{tT}^4 + 60r_{tT}^6 \log r_{tT}^2 - 20r_{tT}^6 - 30r_{tT}^8 + 3r_{tT}^{10}}{180(1 - r_{tT}^2)^6}. \tag{39}
\end{aligned}$$

Keeping the terms up to $\mathcal{O}(\frac{1}{m_T^4})$ and considering the $\log r_{tT}^2$ enhanced terms, they can be simplified

as

$$\begin{aligned} C_0^{Tt}(\hat{t}) &\approx -\frac{1}{m_T^2} [1 + r_{tT}^2(1 + \log r_{tT}^2) + \frac{m_h^2 + \hat{t}}{4m_T^2}], \\ C_0^{Tt}(m_h^2) &\approx -\frac{1}{m_T^2} [1 + r_{tT}^2(1 + \log r_{tT}^2) + \frac{\hat{s}}{12m_T^2} + \frac{m_h^2}{2m_T^2}]. \end{aligned} \quad (40)$$

A.3. Heavy quark expansion of D_0 function

D_0 function is defined as:

$$\begin{aligned} D_0(k_1^2, k_{12}^2, k_{23}^2, k_3^2, k_2^2, k_{13}^2, m_0^2, m_1^2, m_2^2, m_3^2) \\ \equiv \frac{(2\pi\mu)^{4-D}}{i\pi^2} \int d^D q \frac{1}{(q^2 - m_0^2)[(q+k_1)^2 - m_1^2][(q+k_2)^2 - m_2^2][(q+k_3)^2 - m_3^2]} \\ = \int_0^1 \int_0^1 \int_0^1 \int_0^1 dx dy dz dw \frac{\delta(x+y+z+w-1)}{[xm_0^2 + ym_1^2 + zm_2^2 + wm_3^2 - xyk_1^2 - xzk_2^2 - xwk_3^2 - yzk_{12}^2 - ywk_{13}^2 - zwk_{23}^2]^2}, \end{aligned} \quad (41)$$

where we have $k_{12} \equiv k_1 - k_2$, $k_{23} \equiv k_2 - k_3$, and $k_{13} \equiv k_1 - k_3$. When the four internal masses are all equal, D_0 function can be expanded as [77]

$$\begin{aligned} D_0(k_1^2, k_{12}^2, k_{23}^2, k_3^2, k_2^2, k_{13}^2, m_t^2, m_t^2, m_t^2, m_t^2) \\ = \int_0^1 \int_0^1 \int_0^1 \int_0^1 dx dy dz dw \frac{\delta(x+y+z+w-1)}{[m_t^2 - xyk_1^2 - xzk_2^2 - xwk_3^2 - yzk_{12}^2 - ywk_{13}^2 - zwk_{23}^2]^2} \\ = \frac{1}{6m_t^4} \left[1 + \frac{k_1^2 + k_{12}^2 + k_{23}^2 + k_3^2 + k_2^2 + k_{13}^2}{10m_t^2} + \frac{1}{140m_t^4} (2(k_1^4 + k_2^4 + k_3^4 + k_1^2k_2^2 + k_1^2k_3^2 + k_2^2k_3^2) \right. \\ \left. + 2(k_{12}^4 + k_{13}^4 + k_{23}^4 + k_{12}^2k_{13}^2 + k_{12}^2k_{23}^2 + k_{13}^2k_{23}^2) + 2k_1^2(k_{12}^2 + k_{13}^2) + 2k_2^2(k_{12}^2 + k_{23}^2) + 2k_3^2(k_{13}^2 + k_{23}^2) \right. \\ \left. + (k_1^2k_{23}^2 + k_2^2k_{13}^2 + k_3^2k_{12}^2)) + \mathcal{O}(\frac{k^6}{m_t^6}) \right]. \end{aligned} \quad (42)$$

Especially, we have the following results

$$\begin{aligned} D_0^t(\hat{t}, \hat{s}) &\approx \frac{1}{6m_t^4} \left[1 + \frac{2m_h^2 + \hat{s} + \hat{t}}{10m_t^2} + \frac{6m_h^4 + 4m_h^2(\hat{s} + \hat{t}) + 2\hat{s}^2 + 2\hat{t}^2 + \hat{s}\hat{t}}{140m_t^4} \right], \\ D_0^t(\hat{t}, \hat{u}) &\approx \frac{1}{6m_t^4} \left[1 + \frac{2m_h^2 + \hat{t} + \hat{u}}{10m_t^2} + \frac{5m_h^4 + 4m_h^2(\hat{t} + \hat{u}) + 2\hat{t}^2 + 2\hat{u}^2 + \hat{t}\hat{u}}{140m_t^4} \right]. \end{aligned} \quad (43)$$

The expansion of $D_0^t(\hat{u}, \hat{s})$ can be obtained when replacing the \hat{t} in $D_0^t(\hat{t}, \hat{s})$ by \hat{u} . The expansion of D_0^T functions can be obtained when replacing the m_t in D_0^t by m_T .

When three internal masses are equal, D_0 function can be expanded as

$$\begin{aligned}
& D_0(k_1^2, k_{12}^2, k_{23}^2, k_3^2, k_2^2, k_{13}^2, m_T^2, m_t^2, m_t^2, m_t^2) \\
&= \int_0^1 \int_0^1 \int_0^1 \int_0^1 dx dy dz dw \frac{\delta(x+y+z+w-1)}{[xm_T^2 + (y+z+w)m_t^2 - xyk_1^2 - xzk_2^2 - xwk_3^2 - yzk_{12}^2 - ywk_{13}^2 - zwk_{23}^2]^2} \\
&= \int_0^1 \int_0^1 \int_0^1 \int_0^1 dx dy dz dw \frac{\delta(x+y+z+w-1)}{[xm_T^2 + (y+z+w)m_t^2]^2} \left[1 + \frac{2(xyk_1^2 + xzk_2^2 + xwk_3^2 + yzk_{12}^2 + ywk_{13}^2 + zwk_{23}^2)}{xm_T^2 + (y+z+w)m_t^2} \right] + \mathcal{O}\left(\frac{k^4}{m_{t,T}^8}\right) \\
&\approx \frac{1}{m_T^4} \cdot \frac{1 + 2r_{tT}^2 \log r_{tT}^2 - r_{tT}^4}{2r_{tT}^2(1 - r_{tT}^2)^3} + \frac{(k_1^2 + k_2^2 + k_3^2)}{m_T^6} \cdot \frac{1 + 6r_{tT}^2(1 + r_{tT}^2) \log r_{tT}^2 + 9r_{tT}^2 - 9r_{tT}^4 - r_{tT}^6}{6r_{tT}^2(1 - r_{tT}^2)^5} \\
&\quad + \frac{(k_{12}^2 + k_{23}^2 + k_{13}^2)}{m_T^6} \cdot \frac{1 - 8r_{tT}^2 - 12r_{tT}^4 \log r_{tT}^2 + 8r_{tT}^6 - r_{tT}^8}{24r_{tT}^4(1 - r_{tT}^2)^5}. \tag{44}
\end{aligned}$$

We only expand it up to $\mathcal{O}\left(\frac{k^2}{m_{t,T}^6}\right)$, because the general results will be quite lengthy. For the integral $D_0^{tT}(\hat{t}, \hat{s})$, we obtain the expression up to $\mathcal{O}\left(\frac{k^4}{m_{t,T}^8}\right)$

$$\begin{aligned}
D_0^{tT}(\hat{t}, \hat{s}) &= \int_0^1 \int_0^1 \int_0^1 \int_0^1 dx dy dz dw \frac{\delta(x+y+z+w-1)}{[xm_T^2 + (y+z+w)m_t^2 - x(y+w)m_h^2 - xzt - yws]^2} \\
&= \int_0^1 \int_0^1 \int_0^1 \int_0^1 dx dy dz dw \frac{\delta(x+y+z+w-1)}{[xm_T^2 + (y+z+w)m_t^2]^2} \\
&\quad \left(1 + \frac{2[x(y+w)m_h^2 + xzt + yws]}{xm_T^2 + (y+z+w)m_t^2} + \frac{3[x(y+w)m_h^2 + xzt + yws]^2}{[xm_T^2 + (y+z+w)m_t^2]^2} \right) + \mathcal{O}\left(\frac{1}{m_{t,T}^{10}}\right) \\
&\approx \frac{1}{m_T^4} \cdot \frac{1 + 2r_{tT}^2 \log r_{tT}^2 - r_{tT}^4}{2r_{tT}^2(1 - r_{tT}^2)^3} + \frac{(2m_h^2 + \hat{t})}{m_T^6} \cdot \frac{1 + 6r_{tT}^2(1 + r_{tT}^2) \log r_{tT}^2 + 9r_{tT}^2 - 9r_{tT}^4 - r_{tT}^6}{6r_{tT}^2(1 - r_{tT}^2)^5} \\
&\quad + \frac{\hat{s}}{m_T^6} \cdot \frac{1 - 8r_{tT}^2 - 12r_{tT}^4 \log r_{tT}^2 + 8r_{tT}^6 - r_{tT}^8}{24r_{tT}^4(1 - r_{tT}^2)^5} + \frac{\hat{s}^2}{m_T^8} \cdot \frac{1 - 9r_{tT}^2 + 45r_{tT}^4 - 45r_{tT}^8 + 9r_{tT}^{10} - r_{tT}^{12} + 60r_{tT}^6 \log r_{tT}^2}{180r_{tT}^6(1 - r_{tT}^2)^7} \\
&\quad + \frac{\hat{s}(\hat{t} + 4m_h^2)}{m_T^8} \cdot \frac{1 - 15r_{tT}^2 - 80r_{tT}^4 + 80r_{tT}^6 + 15r_{tT}^8 - r_{tT}^{10} - 60r_{tT}^4(1 + r_{tT}^2) \log r_{tT}^2}{120r_{tT}^4(1 - r_{tT}^2)^7} \\
&\quad + \frac{\hat{t}^2 + 2m_h^2\hat{t} + 3m_h^4}{m_T^8} \cdot \frac{1 + 28r_{tT}^2 - 28r_{tT}^6 - r_{tT}^8 + 12r_{tT}^2(1 + 3r_{tT}^2 + r_{tT}^4) \log r_{tT}^2}{12r_{tT}^2(1 - r_{tT}^2)^7}. \tag{45}
\end{aligned}$$

Keeping the terms up to $\mathcal{O}\left(\frac{1}{m_T^6}\right)$ and considering the $\log r_{tT}^2$ enhanced terms, they can be simplified as

$$\begin{aligned}
D_0^{tT}(\hat{t}, \hat{s}) &\approx \frac{1}{2m_T^4} \left[\frac{1}{r_{tT}^2} + 3 + 2 \log r_{tT}^2 + r_{tT}^2(5 + 6 \log r_{tT}^2) \right] + \frac{(2m_h^2 + \hat{t})}{6m_T^6} \left(\frac{1}{r_{tT}^2} + 6 \log r_{tT}^2 + 14 \right) \\
&\quad + \frac{\hat{s}}{24m_T^6} \left(\frac{1}{r_{tT}^4} - \frac{3}{r_{tT}^2} - 12 \log r_{tT}^2 - 25 \right). \tag{46}
\end{aligned}$$

Similarly, we can get the following results

$$\begin{aligned}
D_0^{Tt}(\hat{t}, \hat{s}) &\approx \frac{1}{m_T^4} \cdot \frac{1 + 2r_{tT}^2 \log r_{tT}^2 - r_{tT}^4}{2(1 - r_{tT}^2)^3} + \frac{(2m_h^2 + \hat{t})}{m_T^6} \cdot \frac{1 + 9r_{tT}^2 + 6r_{tT}^2(1 + r_{tT}^2) \log r_{tT}^2 - 9r_{tT}^4 - r_{tT}^6}{6(1 - r_{tT}^2)^5} \\
&+ \frac{\hat{s}}{m_T^6} \cdot \frac{1 - 8r_{tT}^2 - 12r_{tT}^4 \log r_{tT}^2 + 8r_{tT}^6 - r_{tT}^8}{24(1 - r_{tT}^2)^5} + \frac{\hat{s}^2}{m_T^8} \cdot \frac{1 - 9r_{tT}^2 + 45r_{tT}^4 - 45r_{tT}^8 + 9r_{tT}^{10} - r_{tT}^{12} + 60r_{tT}^6 \log r_{tT}^2}{180(1 - r_{tT}^2)^7} \\
&+ \frac{\hat{s}(\hat{t} + 4m_h^2)}{m_T^8} \cdot \frac{1 - 15r_{tT}^2 - 80r_{tT}^4 + 80r_{tT}^6 + 15r_{tT}^8 - r_{tT}^{10} - 60r_{tT}^4(1 + r_{tT}^2) \log r_{tT}^2}{120(1 - r_{tT}^2)^7} \\
&+ \frac{\hat{t}^2 + 2m_h^2\hat{t} + 3m_h^4}{m_T^8} \cdot \frac{1 + 28r_{tT}^2 - 28r_{tT}^6 - r_{tT}^8 + 12r_{tT}^2(1 + 3r_{tT}^2 + r_{tT}^4) \log r_{tT}^2}{12(1 - r_{tT}^2)^7}.
\end{aligned} \tag{47}$$

Keeping the terms up to $\mathcal{O}(\frac{1}{m_T^6})$ and considering the $\log r_{tT}^2$ enhanced terms, they can be simplified as

$$D_0^{Tt}(\hat{t}, \hat{s}) \approx \frac{1}{2m_T^4}(1 + 3r_{tT}^2 + 2r_{tT}^2 \log r_{tT}^2) + \frac{2m_h^2 + \hat{t}}{6m_T^6} + \frac{\hat{s}}{24m_T^6}. \tag{48}$$

When two internal masses are equal individually, we have the following relations

$$\begin{aligned}
D_0(k_1^2, k_{12}^2, k_{23}^2, k_3^2, k_2^2, k_{13}^2, m_t^2, m_T^2, m_t^2, m_T^2) &= D_0(k_1^2, k_3^2, k_{23}^2, k_{12}^2, k_{13}^2, k_2^2, m_T^2, m_t^2, m_t^2, m_T^2) \\
&= D_0(k_{23}^2, k_3^2, k_1^2, k_{12}^2, k_2^2, k_{13}^2, m_T^2, m_t^2, m_t^2, m_T^2).
\end{aligned} \tag{49}$$

D_0 function can be expanded as

$$\begin{aligned}
&D_0(k_1^2, k_{12}^2, k_{23}^2, k_3^2, k_2^2, k_{13}^2, m_t^2, m_T^2, m_t^2, m_T^2) \\
&= \int_0^1 \int_0^1 \int_0^1 \int_0^1 dx dy dz dw \frac{\delta(x + y + z + w - 1)}{[(y + z)m_T^2 + (x + w)m_t^2 - xyk_1^2 - xzk_2^2 - xwk_3^2 - yzk_{12}^2 - ywk_{13}^2 - zwk_{23}^2]^2} \\
&= \int_0^1 \int_0^1 \int_0^1 \int_0^1 dx dy dz dw \frac{\delta(x + y + z + w - 1)}{[(y + z)m_T^2 + (x + w)m_t^2]^2} [1 + \frac{2(xyk_1^2 + xzk_2^2 + xwk_3^2 + yzk_{12}^2 + ywk_{13}^2 + zwk_{23}^2)}{(y + z)m_T^2 + (x + w)m_t^2}] + \mathcal{O}(\frac{k^4}{m_{t,T}^8}) \\
&\approx -\frac{1}{m_T^4} \cdot \frac{2 + (1 + r_{tT}^2) \log r_{tT}^2 - 2r_{tT}^2}{(1 - r_{tT}^2)^3} - \frac{k_1^2 + k_2^2 + k_{13}^2 + k_{23}^2}{m_T^6} \cdot \frac{3 + (1 + 4r_{tT}^2 + r_{tT}^4) \log r_{tT}^2 - 3r_{tT}^4}{2(1 - r_{tT}^2)^5} \\
&+ \frac{k_3^2}{m_T^6} \cdot \frac{1 + 6r_{tT}^2(1 + r_{tT}^2) \log r_{tT}^2 + 9r_{tT}^2 - 9r_{tT}^4 - r_{tT}^6}{6r_{tT}^2(1 - r_{tT}^2)^5} + \frac{k_{12}^2}{m_T^6} \cdot \frac{1 + 6r_{tT}^2(1 + r_{tT}^2) \log r_{tT}^2 + 9r_{tT}^2 - 9r_{tT}^4 - r_{tT}^6}{6(1 - r_{tT}^2)^5}.
\end{aligned} \tag{50}$$

We only expand it up to $\mathcal{O}(\frac{k^2}{m_{t,T}^6})$, because the general results will be quite lengthy. For the integral

$D_0^{tT}(\hat{t}, \hat{u})$, we obtain the expression up to $\mathcal{O}(\frac{k^4}{m_{t,T}^8})$

$$\begin{aligned}
D_0^{tT}(\hat{t}, \hat{u}) &= \int_0^1 \int_0^1 \int_0^1 \int_0^1 dx dy dz dw \frac{\delta(x+y+z+w-1)}{[(x+w)m_t^2 + (y+z)m_T^2 - (xy+zw)m_h^2 - xzt - ywu]^2} \\
&= \int_0^1 \int_0^1 \int_0^1 \int_0^1 dx dy dz dw \frac{\delta(x+y+z+w-1)}{[(x+w)m_t^2 + (y+z)m_T^2]^2} \\
&\quad \left(1 + \frac{2[(xy+zw)m_h^2 + xzt + ywu]}{(x+w)m_t^2 + (y+z)m_T^2} + \frac{3[(xy+zw)m_h^2 + xzt + ywu]^2}{[(x+w)m_t^2 + (y+z)m_T^2]^2} \right) + \mathcal{O}(\frac{1}{m_{t,T}^{10}}) \\
&\approx -\frac{1}{m_T^4} \cdot \frac{2 + (1 + r_{tT}^2) \log r_{tT}^2 - 2r_{tT}^2}{(1 - r_{tT}^2)^3} - \frac{2m_h^2 + \hat{t} + \hat{u}}{m_T^6} \cdot \frac{3 + (1 + 4r_{tT}^2 + r_{tT}^4) \log r_{tT}^2 - 3r_{tT}^4}{2(1 - r_{tT}^2)^5} \\
&\quad - \frac{5m_h^4 + 4m_h^2(\hat{t} + \hat{u}) + 2\hat{t}^2 + \hat{t}\hat{u} + 2\hat{u}^2}{m_T^8} \cdot \frac{11 + 27r_{tT}^2 - 27r_{tT}^4 - 11r_{tT}^6 + 3(1 + 9r_{tT}^2 + 9r_{tT}^4 + r_{tT}^6) \log r_{tT}^2}{18(1 - r_{tT}^2)^7}.
\end{aligned} \tag{51}$$

Keeping the terms up to $\mathcal{O}(\frac{1}{m_T^4})$ and considering the $\log r_{tT}^2$ enhanced terms, they can be simplified as

$$D_0^{tT}(\hat{t}, \hat{u}) \approx -\frac{1}{m_T^4} [2 + \log r_{tT}^2 + 4r_{tT}^2(1 + \log r_{tT}^2)] - \frac{4m_h^2 - \hat{s}}{2m_T^6} (3 + \log r_{tT}^2). \tag{52}$$

In the above calculations, the t and T quark mixed C_0 and D_0 integrals will agree with the pure top quark integrals in the limit of $m_t = m_T$ (or $r_{tT} \rightarrow 1$). Besides, these expansion results have been checked by the LoopTools numerically [97].